

Biosignatures of microbial mats in Pleistocene coral reef cores from IODP Expedition 389 (Hawaiian Drowned Reefs)

Hildegard Westphal^{1,2}, Elisa Garuglieri³, Gregory E. Webb⁴, Luke Nothdurft⁵, Anna Merkel⁶, Pankaj Khanna⁷, Poornima Karki⁷, Theresa Nohl⁸, Eberhard Gischler⁹, Jody M. Webster¹⁰

5 ¹Leibniz Centre for Tropical Marine Research, Bremen, Germany

²Department of Geosciences, University of Bremen, Bremen, Germany

³Physical Science and Engineering Division, KAUST, Saudi Arabia

⁴School of the Environment, The University of Queensland, Brisbane, QLD 4072, Australia

10 ⁵School of Earth and Atmospheric Sciences Faculty of Science, Queensland University of Technology, Brisbane, QLD 4000, Australia

⁶GeoZentrum Nordbayern, Friedrich-Alexander-Universität Erlangen-Nürnberg, Germany

⁷Department of Earth Sciences, Indian Institute of Technology Gandhinagar, Department of Earth Sciences, Indian Institute of Technology Gandhinagar, India

⁸University of Vienna, Department of Palaeontology, Vienna, Austria

15 ⁹Institut für Geowissenschaften, Goethe Universität, Frankfurt am Main, Germany

¹⁰Geocoastal Research Group, School of Geosciences, The University of Sydney, NSW 2006, Australia

Correspondence to: Hildegard Westphal (hildegard.westphal@leibniz-zmt.de)

Abstract. We systematically document surfaces and biosignatures of Pleistocene reefal microbialites (Marine Isotope Stages 7-6) recovered during IODP Expedition 389 (Hawaiian Drowned Reefs). Microbialites are abundant within Pleistocene coral reef successions and offer valuable archives of environmental change during Quaternary climate variability. However, relatively little is known about biofilm-forming microbial consortia, because biosignature preservation is usually very poor. The microbial crusts studied here form encrustations as much as 20 cm thick, ranging from laminated to thrombotic, within the coral reef framework. Scanning electron microscopy (SEM) of samples from the windward (humid) Hilo and Kohala and the leeward (arid) Kawaihae sides of the Island of Hawai'i reveals exceptionally well-preserved microbial fabrics that developed during Marine Isotope Stages (MIS) 7-6. Humid side samples exhibit abundant putative calcified exopolymeric substance (EPS) matrices, mineralised filaments, and near spherical, multilobate aggregates that resemble protodolomite spherules formed by modern cyanobacteria or extant coccoid cyanobacteria (e.g., *Gloeocapsa*-type). In either case, the surfaces appear to have been formed with significant aid of cyanobacteria, suggesting formation in a euphotic setting. The microbialites from the arid side display peloidal microfabrics with fewer preserved physical biosignatures, typical of cryptic reefal microbialites, but the surfaces suggest confinement by an organic biofilm. The occurrence of pyrite framboids and huntite-like crystals in the wet-side samples suggests local redox gradients consistent with both sulphate reducing bacteria and cyanobacteria mediating carbonate precipitation. These findings provide the first direct evidence for euphotic microbial mat communities contributing to microbialite formation in Pleistocene drowned Hawaiian reefs, and, to our knowledge, in Indopacific reefs and beyond. The outstanding petrological preservation of calcified EPS and microbial morphotypes

35 highlights the potential of these Pleistocene reefal microbialites as sensitive archives of palaeoenvironmental conditions and
microbial diversity under glacio-eustatic forcing and associated environmental changes.

1 Introduction

Microbialites are organosedimentary deposits formed by benthic microbial communities through processes such as trapping,
binding, and mineral precipitation. They represent some of the most ancient ecosystems in Earth's history and the first to form
40 hard frameworks (Burne and Moore, 1987; Riding et al., 2000a). Their fossil record spans at least 3.5 billion years, providing
insights into early life, biogeochemical cycling, and environmental conditions across geologic time (Grotzinger and Knoll,
1999; Riding et al., 2000b; Riding, 2006; Allwood et al., 2006; Noffke and Awramik, 2026). While marine stromatolites were
globally dominant during the Precambrian and re-emerged prominently following mass extinction events (e.g., the end-
Permian; Schubert and Bottjer, 1992; Baud et al., 1997; Webb, 2005; Pei et al., 2022), other microbialite types were important
45 constituents of skeletal reefs throughout the Phanerozoic (e.g., Pratt, 1982; Webb, 1996). Microbialite occurrence in the
Pleistocene in coral reef-associated, high-diversity, normal marine environments has drawn increasing attention for
understanding carbonate platform dynamics and geomicrobiological processes under Quaternary climate variability (Reid et
al., 2000; Dupraz and Visscher, 2005; Riding et al., 2014; Salas-Saavedra et al., 2022).

Pleistocene reefal microbialites provide archives of environmental change associated with glacio-eustatic and climatic
50 fluctuations, since the microbial communities involved in their formation are highly sensitive to environmental parameters that
affect metabolic processes and marine pH (cf., Riding, 2000b, 2014; Webb and Kamber, 2010). Specifically, Pleistocene reefal
microbialites have been documented across a range of tropical and subtropical carbonate provinces, including the western
Atlantic, Indo-Pacific, Arabian Gulf, and the Red Sea (Camoin et al., 1999; Reitner et al., 2000; Westphal et al., 2010; Heindel
et al., 2012; Braga et al., 2019, among many others). Most, but not all, occurrences are linked to deglacial phases, transgressive
55 reef systems, and possibly lagoonal back-reef environments (White et al., 1984; Camoin et al., 1999; Szilagyí et al., 2020).
Holocene reefal microbialite crusts from Tahiti were interpreted early on as bio-accretionary features (Camoin and
Montaggioni, 1994). In general, such microbialite formation requires: 1) a microbial consortium, 2) an organic carbon source
(a local primary producer acting as energy source for microbial metabolism) that may, or may not, be a major part of the
microbial community, 3) an appropriate nucleation template or scaffold to localize and support mineral precipitation (typically
60 microbial exopolysaccharides - EPS), and 4) a local driver of increased pH and/or alkalinity, generally associated with
microbial metabolism (Castanier et al. 1999; Visscher and Stolz, 2005; Dupraz et al., 2009; Heindel et al., 2010; Webb and
Kamber, 2010; Zhu and Dittrich, 2016; Reid et al., 2024). A general perception exists that the best-known microbialites,
benthic stromatolites, are made by cyanobacteria. Although photosynthetic removal of CO₂ by cyanobacteria and filamentous
green algae can increase pH within benthic biofilms, carbonate precipitation is also driven by processes deeper within the mat,
65 where microbial heterotrophy processes organic matter from the overlying primary producers. Here, heterotrophs can modify
potential nucleation scaffolds (i.e., EPS) and create anoxic microenvironments where sulphate reduction and other

heterotrophic metabolic processes can deeply influence pH, increasing local alkalinity (Castanier et al. 1999; Dupraz et al., 2009; Heindel et al., 2010). The mechanisms involved in microbial carbonate formation within variably confined microenvironments (Dupraz et al., 2009; Webb and Kamber, 2010) are complex, ranging from rather passive calcification of fresh or degraded EPS to mineral precipitation induced by microbial activities (organomineralisation and biologically induced or influenced mineralisation, respectively; e.g., Reitner et al., 1995; Garuglieri et al., 2024). In all cases, the higher the ambient CaCO₃ saturation state, the easier it is for microbial carbonate to accumulate (Riding and Liang, 2005), and microbialite mineral precipitation itself may occur only in highly chemically evolved microenvironments very different from the ambient one that surrounds them (e.g., anoxic versus fully oxygenated; Nothdurft et al., 2007). Hence, microbialites represent a combination of biotic and abiotic factors, thus providing a wealth of (paleo)environmentally significant morphological, textural, mineralogical and biogeochemical information (e.g., Riding, 2000b; Riding and Awramik, 2000; Dupraz and Strasser, 2002; Westphal et al., 2010; Webb and Kamber, 2010).

Reefal microbialites have a variety of morphologies and textures including laminated, thrombolitic, or dendritic structures formed mainly in aphotic (Reitner et al., 1995; Webb and Jell, 1997) to euphotic (shaded?) shallow cryptic reef settings (Westphal et al., 2010), while benthic examples occur in deeper fore-reef slope settings (Heindel et al., 2010; Riding, 2011; Braga et al., 2019; Szilagyi et al., 2020). The study of Pleistocene microbialites from Tahiti (IODP Expedition 310) and the Great Barrier Reef (IODP Expedition 325) pointed to sulphate-reducing bacteria as the main drivers of carbonate precipitation in reefal microbialites (Heindel et al., 2009a; Braga et al., 2019). Nevertheless, the roles of differing trophic levels and metabolic pathways for microbialite formation in general have not been unravelled, and many potential variables exist (e.g., benthic versus tight cryptic, and euphotic versus aphotic settings). Of particular interest for the IODP Expedition 389 successions from leeward and windward settings is that microbialites are affected by differing or fluctuating terrigenous sediment and nutrient flux caused by differences in geography and changing climatic (for example on islands with an exposed and a more protected side, such as Lizard Island, GBR: Reitner, 1993; Tahiti: Camoin et al., 1999) and oceanographic conditions (more intense circulation during deglaciation causing upwelling; as observed for example in the northern Great Barrier Reef: Marshall and Davies, 1988). Additionally, changing atmospheric pCO₂ levels greatly affect marine carbonate saturation (Riding et al. 2014; Szilagyi et al., 2020).

A major hindrance to understanding microbialites is that different indicators highlight distinct aspects of microbialite formation. While biomarker analyses in previous studies point to heterotrophic bacteria (i.e., light-independent organisms) steering calcification, microbioerosion patterns in the surfaces of microbialites (Heindel et al., 2009b) and the taxa of interlayered red algae (Westphal et al., 2010) are consistent with euphotic conditions where the primary producers could have been cyanobacteria. Other reef microbialites formed entirely in aphotic crypts (Webb and Jell, 1997; Gischler et al., 2017) where primary producers may have been cryptic sponges and ascidians (Reitner et al., 1995; Braga et al., 2019; Maak et al., 2024). This emphasizes the broad range of environmental requirements and mechanisms for growth of different reefal microbialites, but also highlights an enigmatic gap in the record of possible photoautotrophic bacteria in the microbialites that formed in euphotic conditions; their presence currently can only be hypothesized. The questions remain as to what are the

primary producers in reef microbialite consortia, and what types of communities or bulk metabolisms drive most mineral precipitation? Until we understand those issues, it will be difficult to retrieve all of the potential environmental data that microbialites record.

105 In most microbialites throughout Earth history, the preservation of identifiable microbial remains is generally poor except for calcimicrobes that were common only in Palaeozoic reefs (Webb 1996). In that case, carbonate precipitated on or replaced EPS, thereby preserving microfossils (e.g., the preserved filament sheaths of *Girvanella*; Zhang et al., 2024). However, precipitation may occur only on degraded organic matter and EPS deeper within the mat, thus preserving organic matter that lacks easily identifiable morphology (Reitner et al., 1995). Additionally, continued alkalinity generation beneath the confining active mat may then drive additional precipitation, coarsening original crystals over time and further overprinting any original
110 organic morphology (e.g., Webb et al., 1998). Thus, preservation of microfossils in microbialites is the exception to the rule (Webb and Kamber, 2010). However, where abundant precipitation occurs near the accretionary surface of the mat, recognizable and informative fossilized microbes may be more abundant.

Prior to the drilling of IODP Expedition 389, the reefal microbialites of Hawaii attracted little attention (Webster et al., 2009). Limited to ROV and dredge samples, two microbial fabrics were observed in samples from the top of Hawaiian drowned reefs:
115 peloidal sediment-filled cavities and laminated to clotted micrite crusts, as much as 5 cm thick, in some cases forming digitate stromatolite overgrowths. Both fabrics were interpreted to postdate the deep-water coralline-algal facies (60-120 m), indicating deposition at greater depths as part of the drowning sequence (Webster et al., 2009). High recovery and extremely good core quality of IODP Expedition 389 now allow for a detailed study of the reef components and succession (Webster et al., 2025). The objective of the present study is to explore MIS 7-6 aged (approximately 133-225 kyr, Webster et al., 2025) reefal
120 microbialites, for gaining insights into their architecture and to characterise the microbial contribution to microbialite formation in coral reefs.

2 Study area and material

IODP Expedition 389 aimed to explore the drowned coral reefs on the rapidly subsiding margins of Hawai'i as archives of sea level and climate change (Webster et al., 2023). As a direct result of Hawai'i's rapid and nearly constant subsidence caused
125 by flexure of the oceanic lithosphere (2.5–2.6 m/ky; Watts, 1978; Webster et al., 2009; Puga-Bernabéu et al., 2016), a 100–200 m thick expanded sequence of shallow coral reef-dominated facies is preserved within the terraces off the Hawai'ian coast. Thus, Hawai'ian reefs cover the time intervals leading into, during, and out of the majority of the last five to six glacial cycles (Webster et al., 2023, 2024, 2025). One objective of this expedition was to gain a better understanding of ancient microbial communities within the reefs and their role in reef building. Based on compiled bathymetric data sets, 13 major terraces were
130 identified around the Island of Hawai'i (designated H0–H12 from shallowest to deepest, where “H” is for Hawai'i) (Webster et al., 2009; Puga-Bernabéu et al., 2016; Sanborn et al., 2017; Taylor, 2019). Drilling operations took place from September to November 2023 with a seafloor drill (PROD5), achieving very good recovery (Webster et al., 2024). Besides well-preserved

135 corals, the cores contain a high percentage of microbialites in the coral reef succession, forming crusts as much as 20 cm in thickness and making up a substantial portion of the recovered lithologies (Webster et al., 2025). Here we study the H2 terrace as recovered at Sites M0097, M0102, and M0104 (Fig. 1; Fig. A1). The H2 terrace, with the top dated at 130 kyr, developed primarily during MIS 7-6, before drowning during the transition to MIS 5e (Fig. 2).

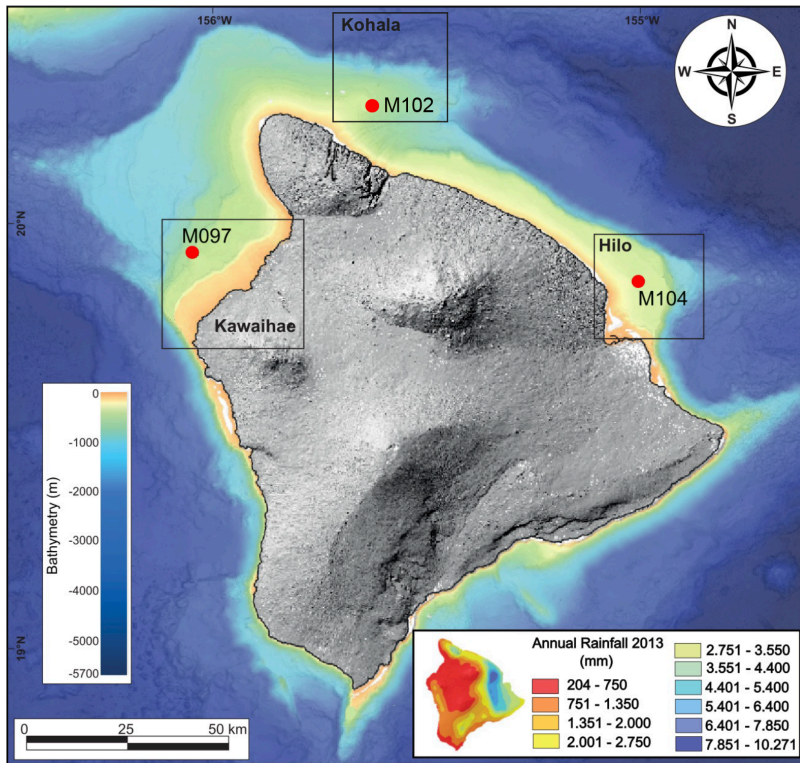
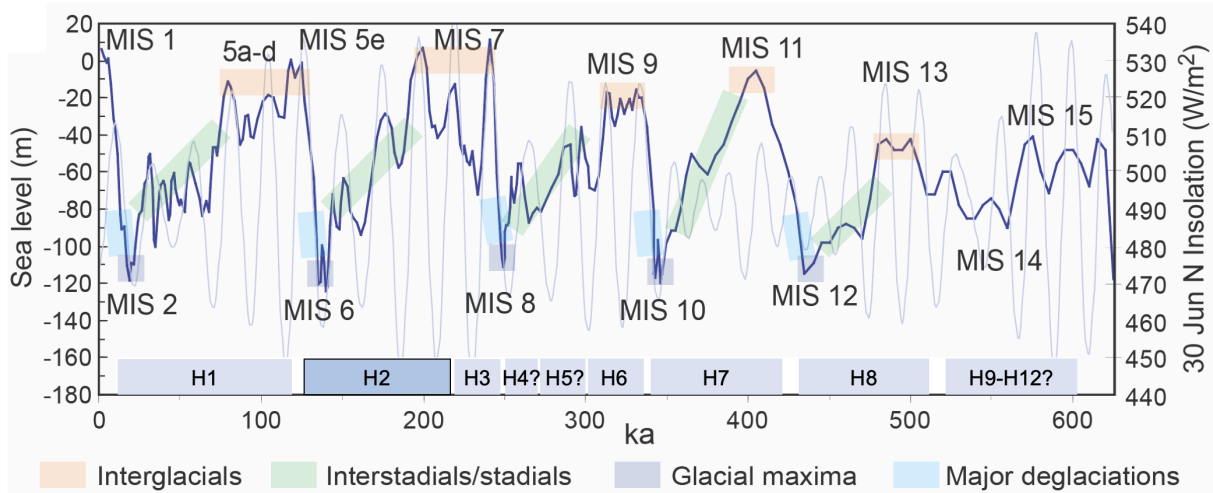


Figure 1: (A) IODP Expedition 389 drill sites M0097, M0102, M0104 studied here; bathymetric map from SOEST (2016; see Webster et al., 2024). Map of modern annual rainfall in the inset (Sanfilippo et al., 2024).



140

Figure 2: Sea level, insolation and reef terraces around the Island of Hawai'i over the last 600 ky (after Imbrie et al., 1984; Berger and Loutre, 1991; Lea et al., 2002). Observational and numerical modelling data indicate that the Hawaiian reef successions (H1–H12) span each interglacial, interstadial/stadial, glacial maxima, and deglacial interval over the past 500-600,000 years with only minor hiatuses (Webster et al., 2009). The present study focuses on the H2 terrace.

145

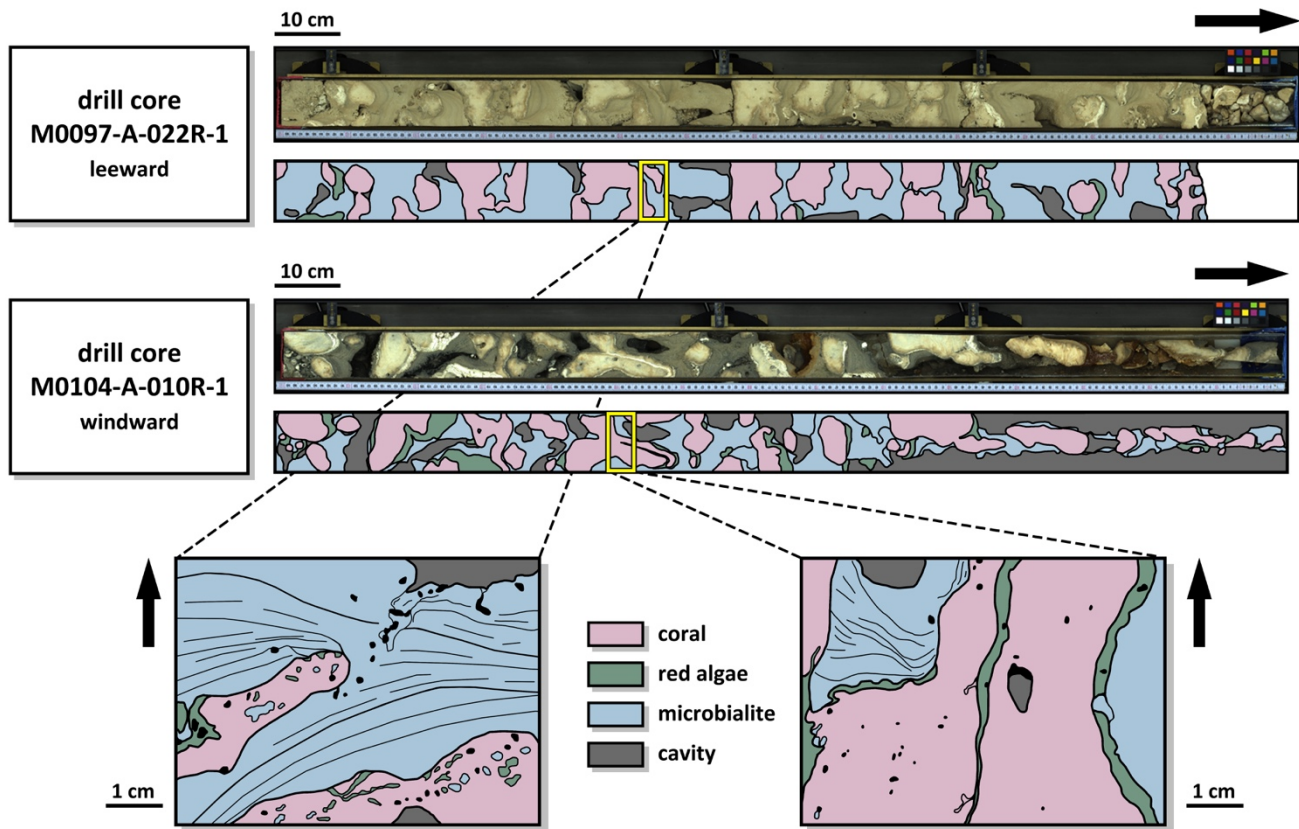


Figure 3: Examples of core section line scans from the arid (M0097-A-022R-1) and humid side (M0104-A-010R-1) of the island of Hawaii, along with the interpretation of coral, encrusting red algae, and microbialite contribution to the reef framework. The close-ups illustrate the occurrence of laminated microbialites within the reef framework.

150 The reefal microbialites in the Hawai’ian succession typically occur as the latest stage of framework sequence, overgrowing the coralgal framework and partly filling cavities in the reef or under ledges created by platy corals (Fig. 3). They form laminated and thrombolitic textures, in most cases occurring on top of red algae crusts that had previously encrusted corals (Webster et al., 2025). This is similar to previously described successions from other locations, such as Tahiti (e.g., Westphal et al., 2010) and the Great Barrier Reef (Braga et al., 2019), where microbialites were interpreted to develop coevally to, or

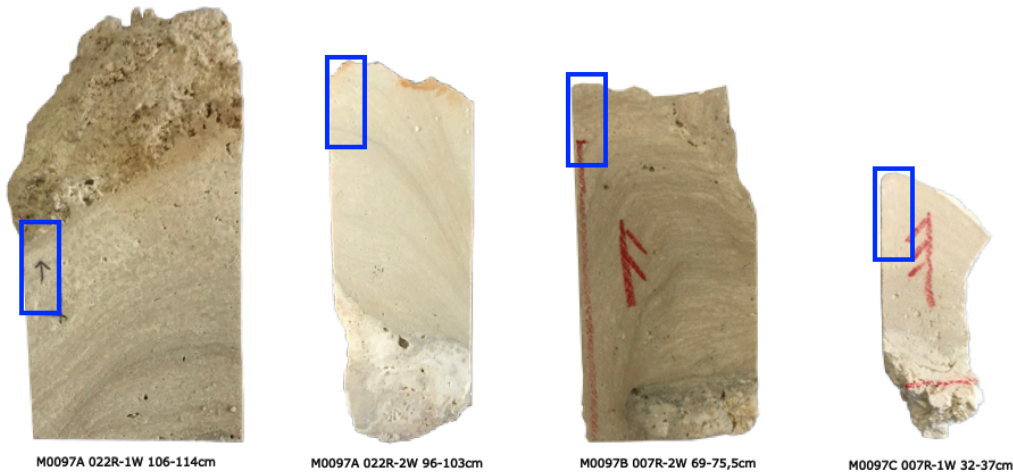
155 immediately after coral growth, while the reef is still in the photic zone (Heindel et al., 2009b; Westphal et al., 2010; Jell and Webb, 2012). Although representing the latest stage of encrustation, these decimetres-thick microbialites do not completely fill the macropore space of the reef framework. In Tahiti, the microbial crusts were estimated to account for as much as 80% of reef rock volume (Séard et al., 2011) and ~43-72% in the IODP 325 cores from the GBR (Szilagyi et al., 2020). As in the Tahitian microbialites, there is a distinct difference in coloration related to humidity and run-off patterns in the Hawai’ian

160 microbialites, with the arid side of the island featuring lighter colours as compared to the humid side (Fig. 2; Fig. A1; Webster et al., 2025).

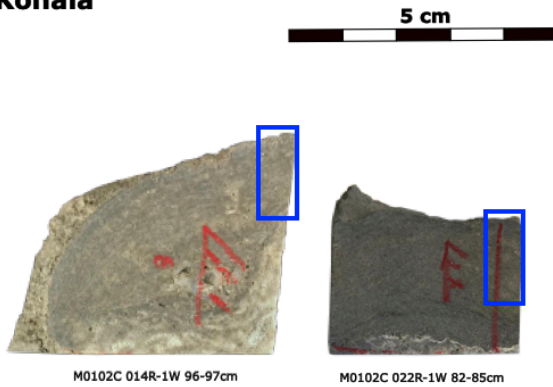
In this study, we compared H2 terrace (MIS7 to MIS6; Webster et al., 2025) microbialites from the windward, humid side of the island (Sites M0102 and M0104) with those from the leeward, dry side (Site M0097) (Fig. 1; Fig. 3; Fig. A1) specifically to identify any morphological biosignatures and document possible differences in microbial signatures between the two settings. A total of seven samples were chosen that have clear, undamaged accretionary surfaces where microbialites grew into reef framework voids, i.e., the final stage of growth (Fig. 4; Table B1). For identifying the microbialites, we followed the criteria of Webb and Kamber (2010), namely the macro-morphology, the micro-morphology, and the appropriate environment (see: Webster et al., 2025), with a special focus on the fourth criterion, i.e., the preservation of morphological bioindicators of microbes as part of the texture.

170

Kawaihae



Kohala



Hilo

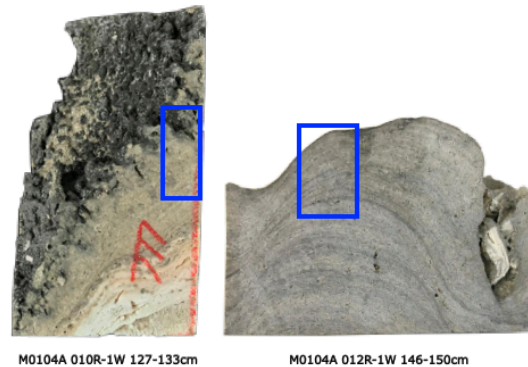


Figure 4: Samples studied by SEM; blue quadrangles indicate the two subsamples prepared for SEM microscopy.

3 Methods

175 Samples were examined under a scanning electron microscope (SEM) to identify microbial features allowing for biological identification. With SEM imaging of microbialite surfaces and vertical polished sections, we characterize the ultrastructure of the crusts and identify trapped and bound particles (e.g., *Cliona* sponge chips from bored reef skeleton; de Bakker et al., 2024) as well as any microbial remains that might allow identification of the microbes, e.g., filaments that are indicative of taxonomic determination (cf., Melim et al., 2015).

180 Prior to analysis, the outermost growth surfaces of microbialites facing voids in the reef edifice were identified. These surfaces were sampled and mounted on SEM stubs. From the same samples, subsamples were cut perpendicular to the laminations and polished with corundum powder (borcarbide 400 and 600). All samples were then cleaned in an ultrasonic bath and rinsed with Millipore water, although in some cases, salts were not entirely removed. Cut samples were then etched with 0.3% (0.1 N) hydrochloric acid for 20 seconds. Note that the preparation, including ultrasonic cleaning as well as the etching of the cut surfaces, prevents contamination. All samples were dried and coated with iridium (10 nm). SEM analysis with a secondary electron (SE) detector was performed with a Teneo-VS SEM at the KAUST Imaging and Characterization Core Lab, and a Tescan Vega LMU at the ZMT Geosciences Laboratory. Element concentrations were measured with an Oxford Energy Dispersive X-ray (EDX X-Max SDD; detector: 50 mm²) coupled to the Tescan Vega LMU. EDX working parameters were set to a beam voltage of 10 kV, a maximum of 5 million counts with a peak pile-up correction, and a process time of 4 min. Dead time was set to 30–50%.

190 X-ray diffraction (XRD) pattern analyses were conducted in the laboratories of the Crystallography and Geomaterials Research Group at the Department of Geosciences, University of Bremen. Dried bulk samples were ground to a fine powder (<20 µm particle size) and prepared with a Philips backloading system. For XRD analysis, a Bruker D8 Discover diffractometer was used. The instrument was equipped with a Cu-tube (k_{α} 1.541 Å, 40 kV, 40 mA), and a fixed divergence slit of ¼°, a monochromatisation via energy discrimination on the highest resolution Linxeye detector system. Measurements were taken as a continuous scan from 3 – 65° 2θ, with a calculated step size of 0.016° 2θ. Mineral identification was done with the Philips software X'Pert HighScore™ Vs. 1.2 (Degen et al., 2014). The determination of well-crystallized minerals like quartz, calcite or aragonite has a standard deviation of ± 1-3 % (Hardy and Tucker, 1988; Vogt et al., 2002).

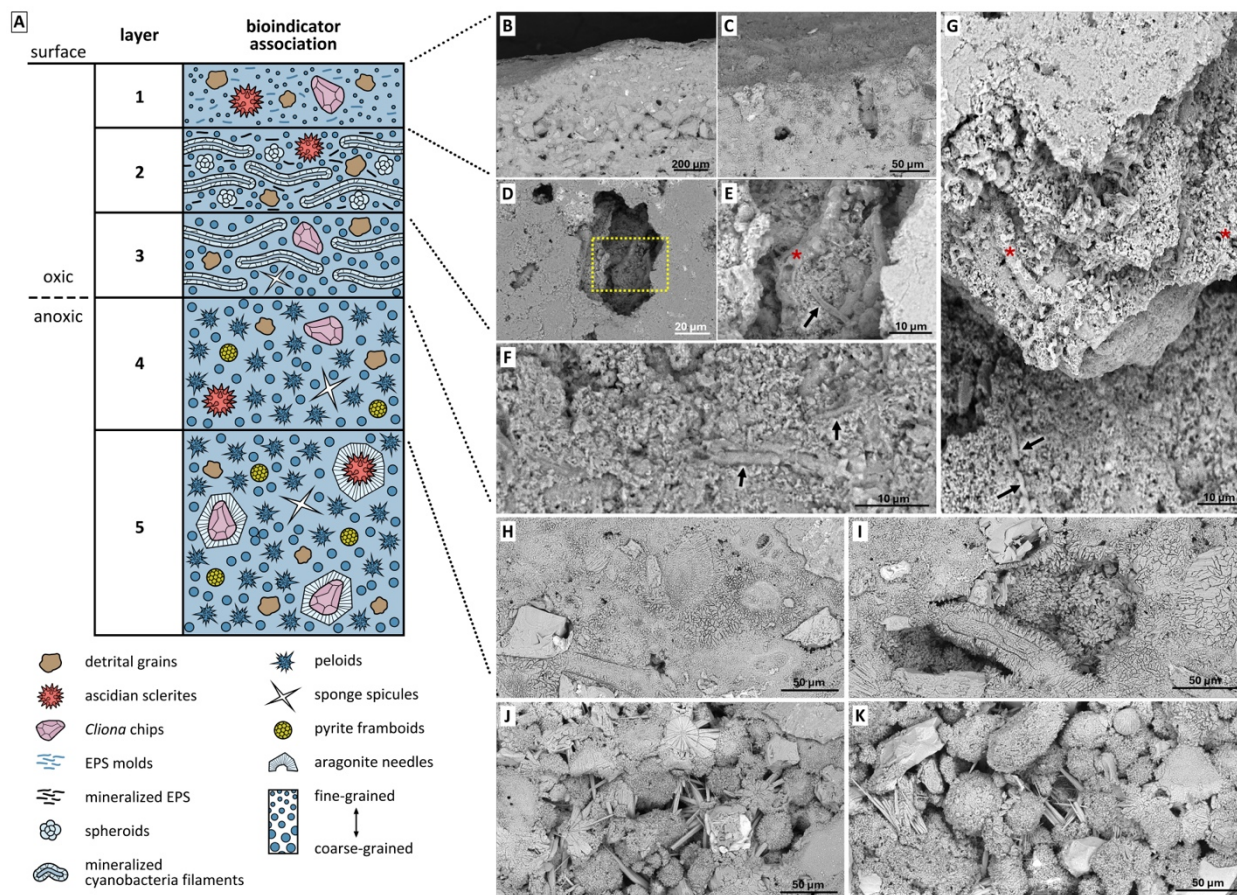
4 Results

4.1 Hilo and Kohala sites - Humid, windward margin

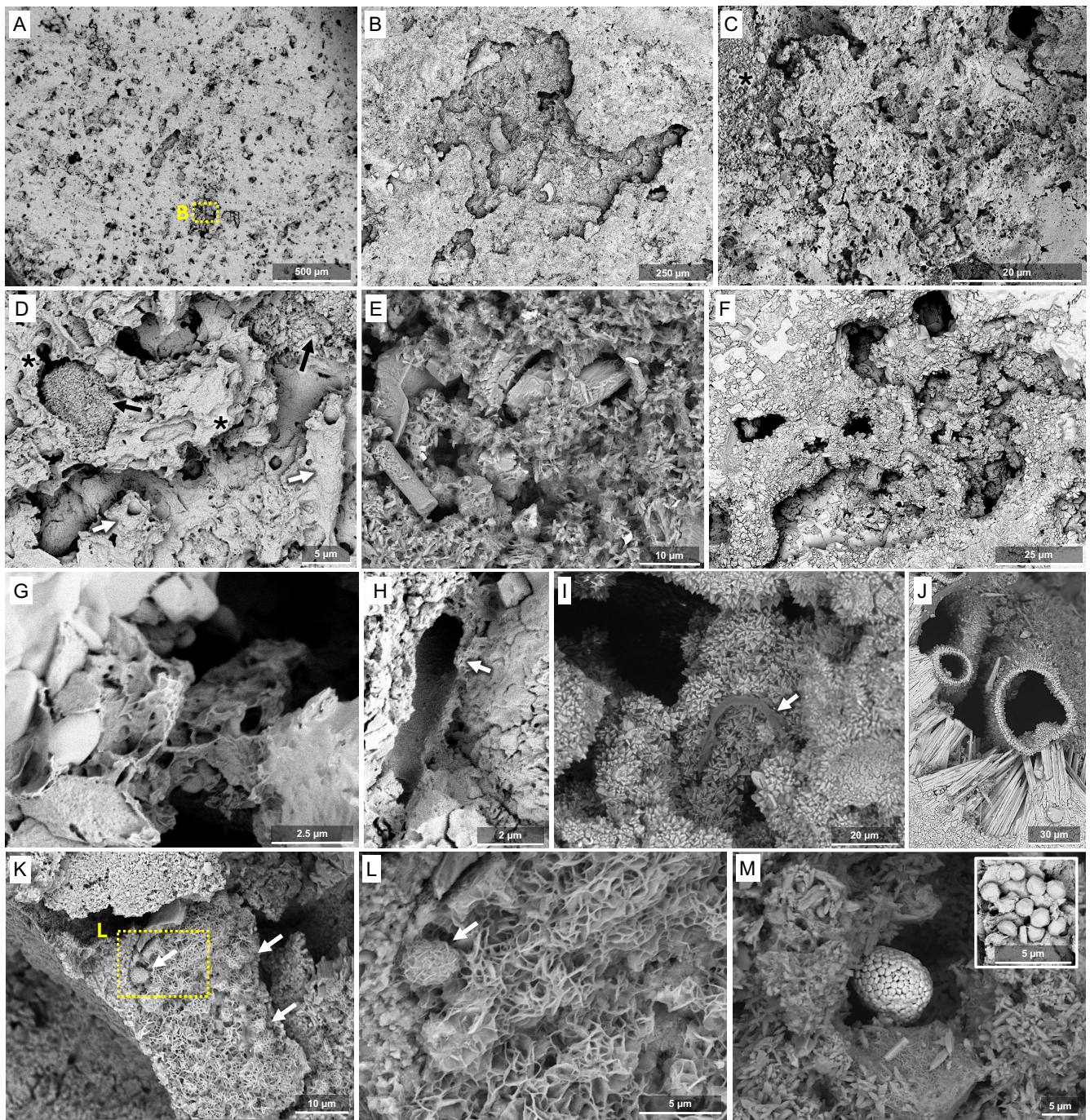
200 The microbialites from the humid side of Hawai'i are organized in layers, five of which can be distinguished on the basis of textures and biomorphic structures (Fig. 5A).

Layer 1 (Fig. 5B, C): The surfaces of the microbialites are smooth, consisting of fine, poorly oriented anhedral crystals (Fig. 6A). This smooth, first layer exhibits a maximum thickness of 1 mm and consistently forms the uppermost element of the

microbialite. The layer shows porous, cracked surfaces, which may represent a modern biofilm that has colonized the older microbialite (Fig. 6A-C). The samples contain abundant trapped and bound skeletal grains (e.g., Fig. 6B, black arrows). At high magnification, the outer layer locally appears to be composed of irregular material showing curved surfaces consistent with mineralised EPS or mucilage residues (Fig. 6D, black asterisks) and hollow filamentous microbial biomorphs emerging from beneath the layer (Fig. 6D, white arrows). Non-carbonate detritus is also present (Fig. 6E) showing an elemental composition pointing to silicates (Fig. C1). Cross-section samples from the windward, humid side of the island (Fig. 6F-J) reveal the deeper layers of the microbialite structure and show that the diffuse porosity observed on the surface continues in the deep with interconnected voids (Fig. 6F).



215 **Figure 5: Typical textures of layers composing microbialites on the humid side of the Island of Hawai'i. (A) Schematic of the five observed layers; (B, C) cut through the surface of the microbialite (Layer 1) showing fine crystalline texture and trapped grains; (D) collapsed surface layer revealing underlying Layer 2; (E) enlargement of Layer 2 showing filamentous biomorphs; (F) Layer 3 with altered and tightly cemented biomorphs; (G) view of Layers 1, 2, and 3 in a broken surface of a microbialite; (H, I) increase in crystal size of cements enclosing trapped and bound grains with cement showing peloidal textures in Layer 4; (J, K) peloidal texture and syntaxial aragonite needle cement on ascidian spicules in Layer 5 samples. Site M0104A, core 12.**



220 Figure 6: SEM images of samples from the humid side of the Island of Hawai'i. (A) Low magnification image of cross-section of the
 fine-crystalline surface. (B) Surface sample showing a collapsed area on the sample surface, revealing underlying Layer 2. (C) Higher
 magnification of the fine-crystalline surface layer material consistent with torn, desiccated, and mineralised EPS. (D) Mineralised
 225 EPS matrix (black asterisks) with mineralised filamentous microbial structures emerging from deeper layers as hollow tubes (white
 arrows), and residual embedded grains (black arrows). (E) Acicular microcrystals. (F) Porous spaces coated by microcrystals. (G)
 Details of torn, laminated matrix-like material consistent with fossilized EPS residues. (H) Hollow calcified sheaths of filamentous

bacteria. (I) Microbial filaments located within a porous space (white arrow). (J) Calcified anastomosed tubes coated with crystals of various dimensions. (K) Flaky precipitates covering spherical biomorphs, (L) close-up of (K). (M) Pyrite aggregates. (E, J, M): Site M0102C, core section 22, all others: Site M0104A, core 12.

230

Layer 2 (Fig. 5D, E): Beneath the outer smooth, fine-crystalline Layer 1, calcified biofilms with preserved filaments occur. A remarkably well-preserved microbial mat shows calcified remains of EPS, isolated and aggregated filaments and a variety of spheroids (Fig. 7). Microbial bioindicators are abundant, including spheroidal and filamentous morphotypes (Fig. 7A-I; black and white arrows, respectively) embedded within the smooth, drape-like matrix. The filamentous morphotypes are horizontally oriented. Globular spheroids of variable size and morphology (Fig. 7B-F; white arrows) are consistently arranged in clustered aggregates. Smaller coccoid forms are also present (Fig. 7D, E). Filamentous structures exhibit a relatively uniform diameter (2–3 μm) and are predominantly preserved as hollow, calcified sheaths.

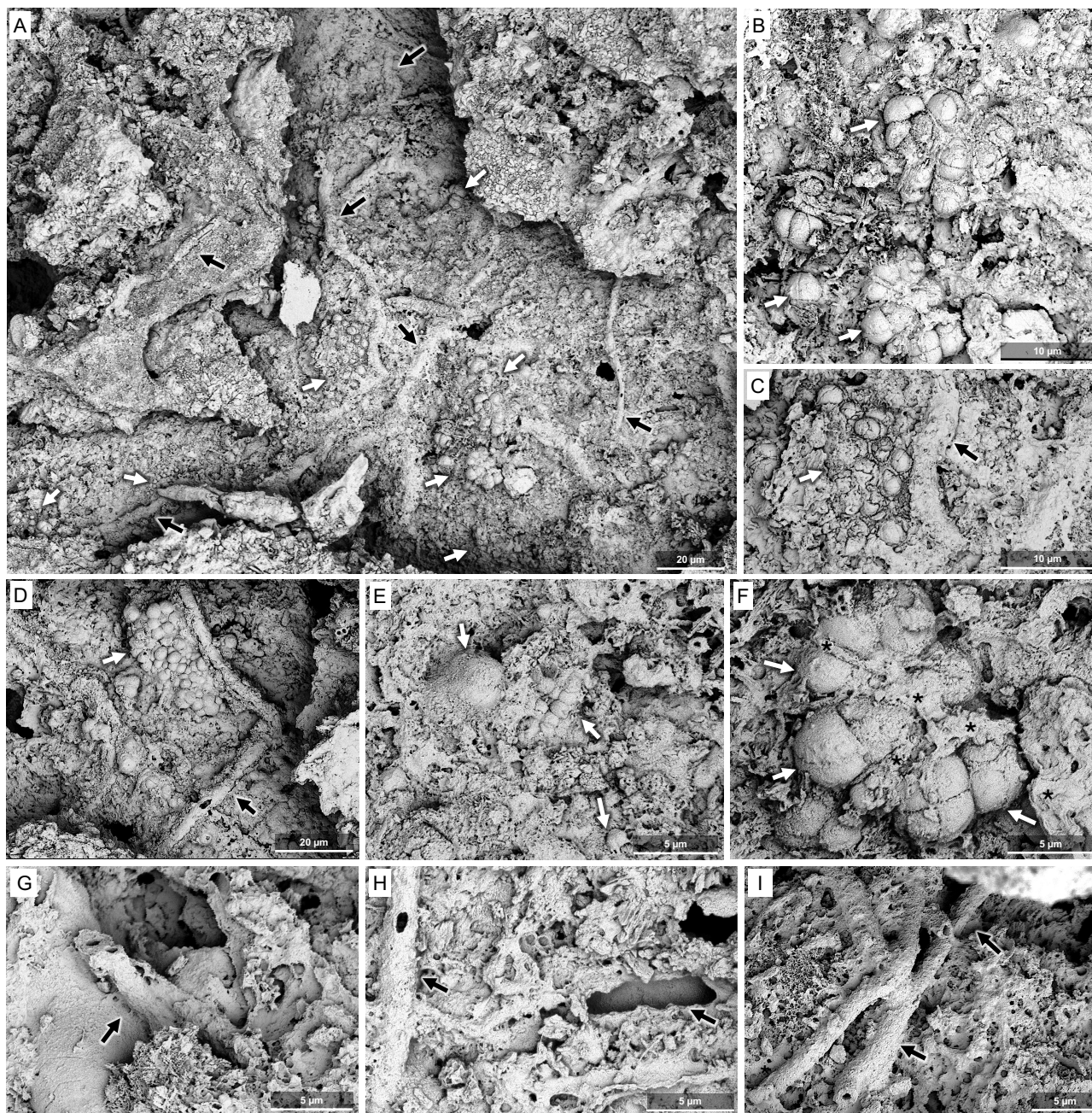
235

Preserved biological structures at the surface include calcified EPS (Fig. 6G), hollow calcified microbial tubes and filaments (Fig. 6H and I, white arrows). The EPS residuals exhibited a filament-rich, matrix-like appearance, similar to that observed on the surface (Fig. 6G). Irregular needle-fibre crystal aggregates are consistent with thin fossilized EPS residuals, possibly at a more degraded stage compared to their surface counterparts (cf., Lin et al., 2019). The voids also contain anastomosed tubes (Fig. 6J). Locally, the tubes and spheroidal morphotypes show an overgrowth of flaky minerals (Fig. 6K, L, white arrows) with elemental composition of Ca, Mg, Al, and Si (Fig. C2).

240

Besides these general features, a remarkably well-preserved microbial mat shows clearly visible calcified EPS residuals, isolated and aggregated filaments and a variety of spheroids (Fig. 7). Microbial bioindicators are abundant, including spheroidal and filamentous morphotypes (Fig. 7A-I; black and white arrows, respectively) embedded within the smooth, drape-like matrix. The filamentous morphotypes are horizontally oriented. Globular spheroids of variable size and morphology (Fig. 7B-F; white arrows) are consistently arranged in clustered aggregates. Smaller coccoid forms are also present (Fig. 7D, E). Filamentous structures exhibit a relatively uniform diameter (2–3 μm) and are predominantly preserved as hollow, calcified sheaths (Fig. 7C, D, G-I, black arrows).

250



255 Figure 7: SEM images of the microbial biofilm (Layer 2) observed on the surface sample from the humid side of the Island of Hawai'i. (A) General view of the crack within the surface layer exposing the biofilm; white arrows indicate coccid biomorphs and black arrows filamentous biomorphs. (B) Details of a group of coccoid biomorphs (white arrows) emerging from copious EPS matrix. (C, D) Details of a group of coccoid structures (white arrow) showing calcified EPS septa (black asterisks) and a filamentous biomorph (black arrow) in two different locations of the biofilm area. The quadrilobed biomorphs are similar to the modern colonial genus *Gleocapsa*. (E) Details of a group of coccoid biomorphs (white arrows) and hollow filaments (black arrow). (F) Details of a group of coccoid biomorphs (white arrows) and abundant EPS in a different spot of the biofilm area. (G-I) Mineralised hollow structures compatible with calcified sheaths of filamentous bacteria (black arrows). All images from Site M0104A, core 12.

260

Layer 3 (Fig. 5F, G): Further below that layer, microbial bioindicators such as filaments appear more altered, calcified and tightly cemented in the matrix.

Layer 4 (Fig. 5H, I): A downward coarsening of the cement crystals is observed in cross-section. Millimetres below the fine-crystalline surface layer, coarser crystals as well as peloidal textures appear (as seen in Fig. 5H, I, 6B, C). Peloidal textures are generally restricted to Layer 4 and below. The matrix encases rare nanocrystal aggregates (average aggregate dimension of 10 μm ; as seen in Fig. 6D black arrows), as well as diffuse microcrystalline areas with irregularly oriented crystals forming peloids or aggregates (as seen in Fig. 6D, E, M) and containing trapped and bound detritus, including arcuate chips of coral skeleton typical for the boring activity of the sponge *Cliona*, abundant ascidian spicules (Fig. 5H) and some calcareous sponge spicules. Pores are typically lined by more euhedral microcrystals (as seen in Fig. 6F, H, I, J). Fine-grained meshes of acicular microcrystals (as seen in Fig. 6E, M) and bladed minerals (as seen in Fig. 6K, L) also occur. Pyrite framboids are present in Layer 4 (Fig. 6M).

Layer 5 (Fig. 5J, K): While otherwise showing the same textural characteristics as Layer 4, in Layer 5, aragonite needle cements are present in Layer 5 as syntaxial overgrowth on aragonitic skeletal grains such as ascidian spicules and coral skeleton cut in chips by the boring sponge *Cliona*.

4.2 Interpretation of Hilo and Kohala sites - Humid, windward margin microbialites

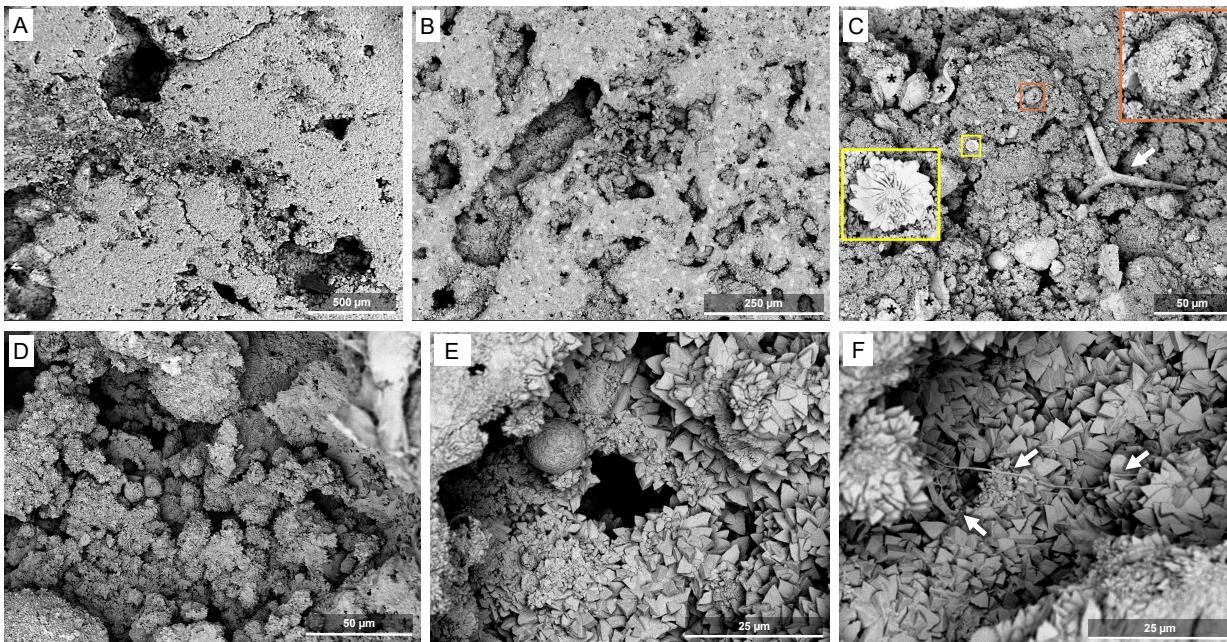
The smooth undulating surface crusts (Layer 1) and increasing euhedral crystal growth as well as intergrown peloids with depth (downwards towards Layer 4, Fig. 5) are consistent with patterns observed in Holocene-modern microbialite growth (Webb et al., 1998). However, the well-preserved filaments and spheroids in Layer 2 with smooth, draping textures suggest abundant precipitation within the surface community where EPS and microbial sheaths were replaced by CaCO_3 (Webb and Kamber, 2010, their Figure 2). The large filament diameter and prostrate growth is consistent with cyanobacteria. The spheroids are more difficult to interpret. Some quadrilobed forms (Fig. 7B, E) closely resemble those observed in extant cyanobacteria of the order Chroococcales (e.g., the genus *Gleocapsa*, of similar dimensions). However, similar features have been produced in cyanobacterial biofilms as protodolomite spheroids, even mimicking a similar lobate morphology (e.g., Zhao et al., 2024).

The great difference in diameter of some of the spheroids in some clusters observed in Layer 2 (Fig. 7D) is more consistent with mineral spheroids, but other clusters are more uniform (Fig. 7B, C, E). The mode of preservation may also favour mineral spheroids, as the filaments are preserved as calcified sheaths left hollow by degradation of the cells within, whereas the spheroids do not appear to be hollow, so would presumably represent preservation of the cells themselves. The large difference in diameter between spheroids of different clusters (Fig. 7A) suggests more than one process was operating in any case. Other holes in the EPS are consistent with microbial structure moulds. Regardless, both spheroid interpretations suggest the presence of cyanobacteria, so we suggest that the microbialites formed in open crypts with abundant light and adequate nutrients to

support a cyanobacterial community as the primary producer of organic matter. Trapped and bound material still includes evidence of abundant cryptic reef dwellers (sponges and ascidians). Abundant coccoliths also occur, consistent with ambient water rich in nutrients. While precipitation occurred in the top layers within the microbial mat (Layers 1-3), thus preserving the filaments of cyanobacteria (oxygenic photoautotrophs), additional precipitation occurred deeper within the mat (Layer 4), where degraded EPS was possibly still preserved, and heterotrophs continued to increase alkalinity, coarsening microbial peloids and lining cavities with scalenohedra, through the activity of an anoxic community. The flaky precipitates with a silicate composition (Fig. C2) observed on biomorphs (6 O-Q) could represent microbial autochthonous clay minerals. Preservation of pyrite framboids in deeper parts of the microbialite, for example, suggests ongoing sulphate reduction, but other processes, such as ammonification, also could have been important. The occurrence of syntaxial aragonite needle cements on skeletal grains suggests (Layer 5) a highly increased alkalinity allowing for precipitation below the main activity of sulphate-reducing bacteria.

4.3 Kawaihae site – Arid, leeward margin

The samples from the dry side of the island lack the distinctive layers observed on the humid side. While no fossilized microbial mats were observed here, other indicators of microbial activity are abundant. Both the growth surfaces (Fig. 8C, D) and the vertically cut samples (Fig. 8A, B, E, F) show massive and peloidal textures composed of variably sized and typically irregularly oriented microcrystals. Peloidal structures as shown in Figure 8D could have formed late in the microbialite owing to endolithic activity in the pore spaces under the rock surface (cf., Falkenberg et al., 2026). The bulk surface appears to be composed of irregularly overlapping laminae that are relatively smooth and undulose in places and more irregular with abundant trapped and bound sediment in others (Fig. 8C). Micropeloidal textures and confining structures are consistent with a biological origin (Fig. 8D-F) and occur in all samples coalescing to form the mineral matrix with minor trapped and bound detritus including both cryptic calcareous sponge spicules and possibly coccoliths (Fig. 8C). Much of the surface consists of irregular peloidal fabric composed of variably sized, mostly irregularly oriented crystals ranging from finer anhedral to coarser subhedral-euhedral shapes. Rare hollow, spherical structures coated in crystals (Fig. 8C; orange square) and tubular filamentous biomorphs (Fig. 8F) also occur, compatible with calcified bacterial cells and strings. One nannolith with a flowery appearance (Fig. 8C; yellow square) likely represents a coccolith.



320 **Figure 8:** SEM images of samples from the Kawaihae site, i.e., the dry side of the Island of Hawai'i. (A, B) Low magnification
 325 micrographs of the vertically cut sample. (C) Assemblage of structures of possible biological origin found on the surface of the
 sample; torn sheet-like matrices compatible with desiccated EPS (black asterisks), a spherical hollow structure consistent with a
 lithified coccoid microorganism (orange square), a calcareous sponge spicule (white arrow) and a coccolith flowery plate possibly
 affiliated to *Discoasteraceae* (yellow square). (D) Peloidal texture with abundant spheroidal structures coated in fine crystals. (E)
 330 Cavity exposed by the cut, covered in a microcrystalline coat. (F) Filaments consistent with EPS strings, indicated by white arrows
 (F). All images from Site M0097B, core 7.

Vertically cut samples are massive with porous zones serving to demarcate minor layering. Most of the micritic structure is
 composed of merged peloidal texture similar to that on the surface (Fig. 8A, B, E). Trapped and bound detritus is relatively
 330 rare, but includes calcareous sponge spicules and chips excavated by the boring sponge *Cliona* from the skeleton of corals.
 The inner surfaces of voids are lined by coarser, more euhedral crystals (Fig. 8B, E, F) as already described for the surface
 samples. Obvious biological structures and signatures are scarce here, consisting of sparse microfilaments consistent with EPS
 fine strings (Fig. 8F). The presence of some characteristic smooth covers, in particular on the dry side of the islands, in both
 surface samples and cuts, may represent halite or organic matter remobilized during preparation.

335 4.4 Interpretation of Kawaihae site – Dry, leeward margin microbialites

The smooth undulating surfaces are consistent with formation at the base of a biofilm and are similar to other described reefal
 microbialites (Webb et al., 1998). The abundant peloids in deeper parts of the microbialites (millimeters depth) are typical of
 peloidal carbonates long associated with bacterial precipitation (e.g., Chafetz and Buczynski, 1992) and the coarsening of
 crystal texture below the surface is consistent with previous observations in reefal microbialites (Webb et al., 1998). The
 340 abundant holes or niches may have been colonized by endolithic microbial colonies, later covered with fine crystals coatings

(cf., Falkenberg et al., 2026). The irregular fine-grained matrix is in places consistent with calcified EPS (Dohlkanova et al., 2011). Trapped and bound material from boring and other cryptic sponges, and the morphology described above is consistent with microbialite formation in semi-enclosed crypts within the reef framework, with no obvious evidence of cyanobacteria.

4.5 Mineralogy

345 Bulk microbialite from both sides consist mainly of high-Magnesium calcite (HMC), making as much as 89% of the samples (Table D1). Aragonite amounts to as much as 15%, while anorthite, i.e., Ca-rich plagioclase, is present (as much as 7%) in samples from the windward side. Traces of quartz, huntite, and other minerals were also observed, but pyrite was not detected, despite framboidal pyrite being found in SEM analysis.

5 Discussion and Conclusions

350 The genesis of reefal microbialites is still not fully understood. While the involvement of cyanobacteria in the formation of microbialites has been discussed for more than a century (e.g., Holtedahl, 1919), it became clear that complex consortia forming microbial mats and creating a succession of microbial activity are involved (e.g. Stolz et al., 2009). As Webb (2005) pointed out, microbialites are not necessarily the product of certain taxa but rather of a diverse consortium of autotrophic and heterotrophic microbes. Nevertheless, previous studies of Pleistocene reefal microbialites remained inconclusive regarding the
355 presence of cyanobacteria (e.g., Heindel et al., 2009a).

The IODP Expedition 389 samples studied here resemble those presented in earlier studies (Heindel et al., 2010; Riding, 2011; Braga et al., 2019; Szilagyi et al., 2020) including the predominant composition of HMC and the textures observed in deeper parts of the microbialite, including the abundance of *Cliona* chips, originating from coral skeletons, as reflected, together with some cements, in the aragonite portion reaching 15% of the bulk microbialite. However, in contrast to reefal microbialites
360 studied earlier, the Hawai’ian microbialites exhibit an extraordinary preservation of microbial mats, featuring cyanobacterial bioindicators. In particular, the samples from the humid side of the Island of Hawai’i show rich bioindicative petrological features. The abundant occurrence of desiccated, cracked and calcified EPS or mucilage residues in surface samples indicates that they indeed are ancient features and have a distinctly different appearance than scattered spots of younger organic material accumulated during preparation on surfaces and cuts. This is also confirmed by the presence of degraded EPS signatures within
365 the rock as exposed in vertical cuts of the samples.

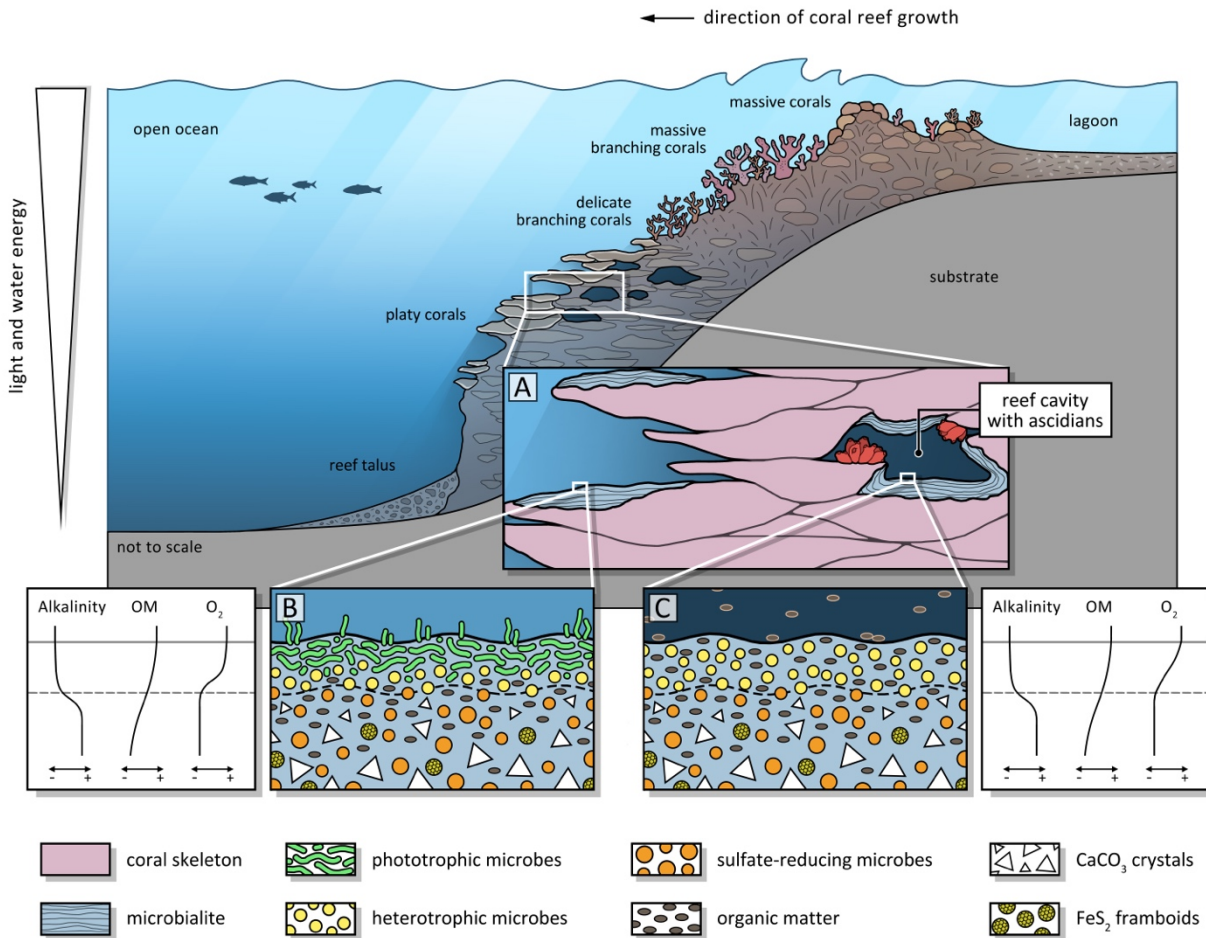
IODP 389 microbialite samples reveal a succession of textures and bioindicators allowing for reconstruction of the successive microbial activities in the succeeding layers (Fig. 5). Figure 7 shows a microbialite surface from the humid side that exhibits a specifically copious and well-preserved layer of calcified EPS. The calcified EPS and biofilm show a “cracked” appearance of the uppermost layer of the surface specimen which, at closer look, is made of torn EPS matrix embedding hollow filamentous
370 sheaths. In the same specimens, pyrite aggregates indicate a reducing micromilieu, caused by heterotrophic oxygen removal, that allowed sulphate reduction within and/or beneath the microbial mats and the formation of local redox gradients. This is

consistent with the findings of Gomes et al. (2021) who showed microbial communities are likely to play a major role in promoting pyrite formation at the surface of microbial mats. The origin of traces of quartz identified in XRD measurements of samples from the windward side of the island is inconclusive. It may be autochthonous, representing remineralised diatom and siliceous sponge skeletons, or may be allochthonous sourced from Asian eolian dust as identified previously on Hawai'i (Kurtz et al., 2001). Quartz was not observed directly in SEM, so its morphology remains unknown.

The observed biofilm areas (Fig. 5-7) are particularly well-preserved and allow characterization of a succession from fine-crystalline, smooth surface layers to “deeper” layers of the biofilm, followed by even deeper and more crystallized layers. Filaments that extend into the embedding EPS and sediments exclude their being modern contaminants. The putative coccoid colonies are also completely embedded in the matrix, which shows the typical appearance of dehydrated EPS with calcified septa in some cell clusters. These spectacular microbial mats with diverse cell types (no bacilli, only globular/cocci and filamentous) and colonies support the hypothesis of an actual microbial multispecies biofilm or microbial mat, some of them consistent with cyanobacteria indicating that the microbialite originated in the photic zone.

In the samples from the arid side of the Island of Hawai'i, discrete layers of biomats were not identified, but similar biosignatures are present, albeit less abundant than on the humid side. Also, fewer spicules of ascidians were identified. Encrusting ascidians are common inhabitants of reef cavities as shown for Lizard Island in the GBR, with their aragonitic spicules being incorporated in microbialites (Reitner, 1993). As ascidians thrive in moderate to elevated nutrient levels (e.g., Ribes et al., 2005; Eckhard et al., 2024) a lower abundance on the arid side of the island might be expected.

The flaky and mesh-like minerals observed (Fig. 6O-Q) resemble the magnesium carbonate huntite known from microbialites forming in high-salinity/alkalinity crater lakes (Caumartin et al., 2025), or the magnesium carbonate dypingite that is known to be associated with modern cyanobacteria in alkaline wetlands (Power et al., 2007; Shirokova et al., 2013). It is known that EPS secreted by cyanobacteria can bind Mg^{2+} , creating microenvironments conducive to mineral nucleation (Robles-Fernández et al., 2022). Dypingite, however, does not form in marine waters and has never been confirmed in reefal microbialites. Also, Mg clays can have a similar appearance and are known to form in the context of cyanobacteria (Perri et al., 2017). Therefore, an interpretation remains speculative. However, XRD analyses indicate the presence of traces of huntite, which is known to form in microbialites (Caumartin et al., 2025). The observation that HMC is so ubiquitous in reefal microbialites in general (Reitner, 1993; Camoin et al., 1999; Gischler et al., 2017) and in the Hawai'ian examples studied here in particular lends evidence to the presence of heterotrophic bacteria as well. Sulfate-reducing bacteria apparently exert control on calcium carbonate polymorph mineralogy in that HMC and dolomite precipitation occur preferentially, both in experiments and in a modern coastal lagoon environment (van Lith et al., 2003).



405 **Figure 9: Schematic diagram of loci of microbialite formation in a coral reef under slightly shaded euphotic versus oligophotic cryptic conditions. Section through a coral reef, (A) euphotic versus cryptic setting in a cavity, (B) close-up of euphotic setting with cyanobacterial mat at the surface of the microbialite, (C) close-up of detrital organic matter-driven microbial mat in a cavity. Diagrams illustrating gradients in alkalinity, organic matter, and oxygen throughout the upper layers of the microbial mats.**

Evidence found in the MIS 7-6 wet-side microbialite samples from IODP 389 allows us to reconstruct the microbialites as the product of photic biomats that featured abundant cyanobacteria, while a few millimeters below this exposed surface, sulphate reducing and other heterotrophic microbes are suspected to drive larger scale calcification, producing peloidal textures typical for microbialites, and evidenced by pyrite framboids (Fig. 5). They seem to drive oversaturation of the porewater with respect to HMC as evidenced in the peloidal texture, and with aragonite in deeper layers of the microbialite where it precipitates as syntaxial needle cement. While this model seems conclusive for the humid, windward side of the island, its applicability on the arid side is not fully coherent, because the bioindicators of cyanobacteria have not been found. The question remains open as to why the record recovered on the humid side of the Island of Hawai'i contains such well-preserved cyanobacterial traces compared to the arid side, as well as to the substantially younger, last deglacial successions recovered in Tahiti (IODP 310)

410

415

and the glacial maximum to deglacial aged ones from the GBR (IODP 325) (Westphal et al., 2010; Braga et al. 2019). The microbialites lacking cyanobacterial remains could represent a fully cryptic, aphotic setting where cyanobacteria did not thrive. Figure 9 schematically illustrates the different environments in a coral reef where microbialites may form under varying photic conditions. While aphotic microbialites are known from modern reef cavities and are typically characterized by abundant sponge or ascidian spicules (Reitner, 1993; Gischler et al., 2017; Maak et al., 2024), in the present study, on the humid side of Hawaii, ascidians cooccur with cyanobacteria, pointing to shaded and more nutrient-rich settings between platy corals in the euphotic zone. For the arid side of Hawaii, either an aphotic cryptic origin of the microbialites or poor preservation of the surface mat could explain the absence of preserved biomorphs. This study emphasizes the point that reefal microbialites represent a diverse set of precipitates that may have different origins in different environmental settings within the reef. Understanding their differences and similarities should render them more useful as environmental archives.

Author contributions

JMW acted as co-chief scientist of expedition IODP 389 and was thus instrumental in designing and conducting the cruise and securing the core material; HW designed the present study; HW prepared the sample material; HW and EGa conducted the SEM and EDX analyses; HW, EGa and GEW interpreted the data with contributions by all authors; AM did the artwork in Figures 5 and 9; HW drafted the first version of the manuscript; all co-authors substantially contributed to the manuscript and the revision.

Competing interests

The authors declare no conflicts of interest.

Acknowledgements

This publication benefitted from reviews by Nora Noffke and Joachim Reitner. We are grateful to Sebastian Flotow for support with the preparation of the samples and operation of the SEM at ZMT. Maximilian Göbel (Bremen University) helped with the preparation of the samples and the SEM work at ZMT. This work is part of the research to fulfil the obligations of the IODP X389 Science party, of which HW, PK, TN, EGa, and JMW are members. We are indebted to the IODP, Bremen Core Repository (MARUM, University of Bremen), and British Geological Service personnel supporting the work on IODP X389.

Financial support

This research was funded by ZMT baseline funding to HW. JMW and GEW acknowledge support provided by the Australian Research Council (Grant No. DP250102180) and ANZIC (Grant No. PCAFX38901).

Review statement

The review statement will be added by Copernicus Publications, listing the handling editor as well as all contributing referees
445 according to their status anonymous or identified.

Data availability

The SEM micrographs and metadata are available from the corresponding author upon request.

References

- Allwood, A.C., Walter, M.R., Kamber, B.S., Marshall, C.P., and Burch, I.W.: Stromatolite reef from the Early Archaean era
450 of Australia. *Nature*, 441(7094), 714–718, 2006.
- Andres, M.S. and Reid, R.P.: Growth morphologies of modern marine stromatolites: a case study from Highborne Cay, Bahamas. *Sedimentary Geology*, 185(3–4), 319–328, 2006.
- Baud, A., Cirilli, S., and Marcoux, J.: Biotic response to mass extinction: the lowermost Triassic microbialites. *Facies*, 36, 238–242, 1997.
- 455 Berger, A. and Loutre, M.F.: Insolation values for the climate of the last 10 million years. *Quaternary Science Reviews*, 10(4):297–317. [https://doi.org/10.1016/0277-3791\(91\)90033-Q](https://doi.org/10.1016/0277-3791(91)90033-Q), 1991.
- Braga, J.C., Puga-Bernabéu, Á., Heindel, K., Patterson, M.A., Birgel, D., Peckmann, J., Sánchez-Almazo, I.M., Webster, J.M., Yokoyama, Y., and Riding, R.: Microbialites in Last Glacial Maximum and deglacial reefs of the Great Barrier Reef (IODP Expedition 325, NE Australia): *Palaeogeography, Palaeoclimatology, Palaeoecology*, v. 514, 1–17, 2019.
- 460 Burne, R. V. and Moore, L. S.: Microbialites: Organosedimentary deposits of benthic microbial communities. *Palaios*, 2(3), 241–254, 1987.
- Camoin, G.F. and Montaggioni, L.: High energy coralg-al-stromatolite frameworks from Holocene reefs (Tahiti, French Polynesia). *Sedimentology*, 41: 655–676, 1994.
- Camoin, G.F., Gautret, P., Montaggioni, L., and Cabioch, G.: Nature and environmental significance of microbialites in
465 Quaternary reefs: the Tahiti paradox. *Sedimentary Geology*, 126: 271–304, 1999.
- de Bakker, D. M., Perry, C. T., Magana-Gallegos, E., Perez-Cervantes, E., and Alvarez-Filip, L.: Fine-grained sediment production by endolithic sponges on Caribbean coral reefs. *Limnology and Oceanography*, 69(9), 2015–2028. <https://doi.org/10.1002/lno.12640>, 2024.
- Degen, T., Sadki, M., Bron, E., König, U., and Nénert, G.: The HighScore suite. *Powder Diffraction*, 29 (S2), S13–S18.
470 doi:10.1017/S0885715614000840, 2014.

- Dohnalkova, A. C., Marshall, M. J., Arey, B. W., Williams, K. H., Buck, E. C., and Fredrickson, J. K.: Imaging hydrated microbial extracellular polymers: comparative analysis by electron microscopy. *Applied and environmental microbiology*, 77(4), 1254-1262, 2011.
- 475 Dupraz, C. and Strasser, A.: Nutritional modes in coral-microbialite reefs (Jurassic, Oxfordian, Switzerland): Evolution of trophic structure as a response to environmental change, *Palaios*, 2002, 17: 449-471, 2002.
- Dupraz, C. and Visscher, P.T.: Microbial lithification in marine stromatolites and hypersaline mats. *Trends in Microbiology*, 13(9), 429-438, 2005.
- Dupraz, C., Reid, R.P., Braissant, O., Decho, A.W., Norman, R.S., and Visscher, P.T.: Processes of carbonate precipitation in modern microbial mats. *Earth-Science Reviews*, 96(3-4), 141-162, 2009.
- 480 Eckhardt, S., Ainsworth, T. D., Leggat, W., and Page, C. E.: Colonial ascidian populations at inshore coral reefs of Norfolk Island, South Pacific. *Diversity*, 16(7), 384, <https://doi.org/10.3390/d16070384>, 2024.
- Expedition 310 Scientists: Expedition 310 summary. In: Camoin GF, Iryu Y, McInroy DB, and the Expedition 310 Scientists. *Proc. IODP, 310: Washington, DC (Integrated Ocean Drilling Program Management International, Inc.)*. <https://doi.org/10.2204/iodp.proc.310.101.2007>, 2007.
- 485 Falkenberg, P., Vahrenkamp, S., Garuglieri, E., Petrovic, A., Hachmann, K., Chandra, V., and Vahrenkamp, V.: Polygonal tepee structures of Arabia. *The Depositional Record*, 12, e70043. <https://doi.org/10.1002/dep2.70043>, 2026.
- Garuglieri, E., Marasco, R., Odobel, C., Chandra, V., Teillet, T., Areias, C., Sánchez-Román, M., Vahrenkamp, V., and Daffonchio, D.: Searching for microbial contribution to micritization of shallow marine sediments. *Environmental Microbiology*, 26(2), e16573, 2024.
- 490 Gischler, E., Heindel, K., Birgel, D., Brunner, B., Reitner, J., and Peckmann, J.: Cryptic biostalactites in a submerged karst cave of the Belize Barrier Reef revisited: pendant bioconstructions cemented by microbial micrite. *Palaeogeography Palaeoecology Palaeoclimatology*, 468, 34-51, 2017.
- Gomes, M.L., Klatt, J.M., Dick, G.J., Grim, S.L., Rico, K.I., Medina, M., Ziebis, W., Kinsman-Costello, L., Sheldon, N.D., and Fike, D.A.: Sedimentary pyrite sulfur isotope compositions preserve signatures of the surface microbial mat environment in sediments underlying low-oxygen cyanobacterial mats. *Geobiology*, 20, 60-78. <https://doi.org/10.1111/gbi.12466>, 2022.
- 495 Grotzinger, J.P. and Knoll, A.H.: Stromatolites in Precambrian carbonates: Evolutionary mileposts or environmental dipsticks? *Annual Review of Earth and Planetary Sciences*, 27, 313-358, 1999.
- Hardy, R.G. and Tucker, M.: X-ray powder diffraction of sediments. In: Tucker, M. (ed.): *Techniques in sedimentology*. 191-228, Oxford Blackwell, 1988.
- 500 Heindel, K., Birgel, D., Brunner, B., Thiel, V., Westphal, H., Gischler, E., Ziegenbalg, S.B., Cabioch, G., Sjövall, P., and Peckmann, J.: Post-glacial microbialite formation in coral reefs in the Pacific, Atlantic, and Indian Ocean. *Chemical Geology* 304-305, 117-130. <https://doi.org/10.1016/j.chemgeo.2012.02.009>, 2012.

- Heindel, K., Birgel, D., Peckmann, J., Kuhnert, H., Westphal, H.: Sulfate-reducing bacteria as major players in the formation of reef-microbialites during the last sea-level rise (Tahiti, IODP 310). *Geochimica et Cosmochimica Acta*, 73 (13), 505 Goldschmidt Conference A514-A514, 2009a.
- Heindel, K., Birgel, D., Peckmann, J., Kuhnert, H., and Westphal, H.: Formation of deglacial microbialites in coral reefs off Tahiti (IODP 310) involving sulfate-reducing bacteria. *Palaios* 25, 618–635. <https://doi.org/10.2110/palo.2010.p10-032r>, 2010.
- Heindel, K., Westphal, H., Wisshak, M.: Bioerosion in the reef framework, IODP Expedition #310 off Tahiti (Tiarei, Mara'a, and Faa'a); In: Camoin, G.F., Iryu, Y., McInroy, D.B., and the Expedition 310 Scientists, *Proceedings IODP, 310*, 28 p. <https://doi.org/10.2204/iodp.proc.310.201.2009>, 2009b.
- Heindel, K., Wisshak, M., Westphal, H.: Microbioerosion in Tahitian reefs: a record of environmental change during the last deglacial sea-level rise (IODP #310). *Lethaia* 42, 322-340. <https://doi.org/10.1111/j.1502-3931.2008.00140.x>, 2009c.
- Holtedahl, O. (1919) The Paleozoic formations of Finmarken in northern Norway. *American Journal of Science*, 4(278), 85-515 107.
- Imbrie, J., Hays, J.D., Martinson, D.G., McIntyre, A., Mix, A.C., Morley, J.J., Pisias, N.G., Prell, W.L., and Shackleton, N.J.: The orbital theory of Pleistocene climate: support from a revised chronology of the marine $\delta^{18}O$ record. *Proceedings of the NATO Advanced Research Workshop*, 1984:269. <https://ui.adsabs.harvard.edu/abs/1984mcur.conf.269I>, 1984.
- Jell, J.S. and Webb, G.E.: Geology of heron island and adjacent reefs, Great Barrier Reef, Australia. *Episodes* 35 (1), 110–520 119, 2012.
- Kahal, A.Y., El-Sorogy, A., Alfaifi, H., Almadani, S., and Kassem, O.: Biofacies and diagenetic alterations of the Pleistocene coral reefs, northwest Red Sea coast, Saudi Arabia. *Geological Journal*, 55, 1380–1390, 2019.
- Kurtz, A.C., Derry, A.D., and Chadwick, O.A.: Accretion of Asian dust to Hawaiian soils: isotopic, elemental, and mineral mass balances, *Geochimica et Cosmochimica Acta*, 65, 1971-1983, [https://doi.org/10.1016/S0016-7037\(01\)00575-0](https://doi.org/10.1016/S0016-7037(01)00575-0), 2001.
- 525 Lambeck, K. and Chappell, J.: Sea level change through the last glacial cycle. *Science*, 292(5517):679–686. <https://doi.org/10.1126/science.1059549>, 2001.
- Lea, D.W., Martin, P.A., Pak, D.K., and Spero, H.J.: Reconstructing a 350 ky history of sea level using planktonic Mg/Ca and oxygen isotope records from a Cocos Ridge core. *Quaternary Science Reviews*, 21(1):283–293. [https://doi.org/10.1016/S0277-3791\(01\)00081-6](https://doi.org/10.1016/S0277-3791(01)00081-6), 2002.
- 530 Lin, F., Zhu, X., Li, J., Yu, P., Luo, Y., and Liu, M.: Effect of extracellular polymeric substances (EPS) conditioned by combined lysozyme and cationic polyacrylamide on the dewatering performance of activated sludge. *Chemosphere*, 235, 679-689, 2019.
- Ludwig, K.R., Szabo, B.J., Moore, J.G., and Simmons, K.R.: Crustal subsidence rate off Hawaii determined from $^{234}U/^{238}U$ ages of drowned coral reefs. *Geology*, 19(2):171–174. [https://doi.org/10.1130/0091-7613\(1991\)019<0171:CSROHD>2.3.CO;2](https://doi.org/10.1130/0091-535 7613(1991)019<0171:CSROHD>2.3.CO;2), 1991.

- Maak, J.M., Birgel, D., Reitner, J., Gischler, E., Dullo, W.C., Foster, W., and Peckmann, J.: Molecular fossils in microbial carbonates and sponges of the deep fore reef of Mayotte and Moheli, Comoro Islands. *Facies*, 70, doi.org/10.1007/s10347-023-00678-3, 2024.
- Marshall, J.F. and Davies, P.J.: *Halimeda* bioherms of the northern Great Barrier Reef. *Coral Reefs*, 6: 139–148, 1988.
- 540 Melim, L.A., Northup, D.E., Spilde, M.N., and Boston, P.J.: Update: Living reticulated filaments from Herbstlabyrinth-Adventhöhle Cave System Germany. *Journal of Cave and Karst Studies* 77(2), 87–90. DOI: 10.4311/2015MB0112, 2015.
- Noffke, N. and Awramik, S.M.: A tale of two microbialites: Stromatolites and microbially induced sedimentary structures. *Sedimentology*. <https://doi.org/10.1111/sed.70109>, 2026.
- Nothdurft, L.D. and Webb, G.E., Bostrom, T., and Rintoul, L.; Calcite-filled borings in the most recently deposited skeleton
545 in live-collected *Porites* (Scleractinia): implications for trace element archives. *Geochimica et Cosmochimica Acta* 71:5423–5438. doi:10.1016/j.gca.2007.09.025, 2007.
- Pei, Y., Hagdorn, H., Voigt, T., Duda, J.-P., and Reitner, J.: Palaeoecological Implications of Lower-Middle Triassic Stromatolites and Microbe-Metazoan Build-Ups in the Germanic Basin: Insights into the Aftermath of the Permian–Triassic Crisis. *Geosciences* 12(3), 133. <https://doi.org/10.3390/geosciences12030133>, 2022.
- 550 Perri, E., Tucker, M.E., Słowakiewicz, M., Whitaker, F., Bowen, L., and Perrotta, I.D.: Carbonate and silicate biomineralization in a hypersaline microbial mat (Mesaieed sabkha, Qatar): Roles of bacteria, extracellular polymeric substances and viruses. *Sedimentology*, 65: 1213–1245. <https://doi.org/10.1111/sed.12419>, 2018.
- Power, I.M., Wilson, S.A., Thom, J.M., Dipple, G.M., and Southam, G.: Biologically induced mineralization of dypingite by cyanobacteria from an alkaline wetland near Atlin, British Columbia, Canada. *Geochem Trans* 8:13, doi:10.1186/1467-4866-
555 8-13, 2007.
- Pratt, B.R.: Stromatolite decline—a reconsideration: *Geology*, v. 10, p. 512–515, 1982.
- Puga-Bernabéu, Á., Webster, J.M., Braga, J.C., Clague, D.A., Dutton, A., Eggins, S., Fallon, S., Jacobsen, G., Paduan, J.B., and Potts, D.C.: Morphology and evolution of drowned carbonate terraces during the last two interglacial cycles, off Hilo, NE Hawaii. *Marine Geology*, 371:57–81. <https://doi.org/10.1016/j.margeo.2015.10.016>, 2016.
- 560 Reid, P., Visscher, T.P., Decho, A.W., Stolz, J.F., Bebout, B.M., Dupraz, C., MacIntyre, I.G., Paerl, H.W., Pinckney, J.L., Prufert-Bebout, L., Steppe, T.F., and DesMarais, D.J.: The role of microbes in accretion, lamination, and early lithification of modern marine stromatolites. *Nature*, 406: 989–992, 2000.
- Reid, R.P., Suosaari, E.P., Oehlert, A.M., Pollier, C.G.L., and Dupraz, C.: Microbialite accretion and growth: lessons from Shark Bay and The Bahamas. *Ann. Rev. Mar. Sci.*, 16, 487–511, 2024.
- 565 Reitner, J.: Modern cryptic microbialite-metazoan facies from Lizard Island (Great Barrier Reef, Australia), formation and concepts. *Facies*, 29: 3–40, 1993.
- Reitner, J., Gautret, P., Marin, F., and Neuweiler, F.: Automicrites in a modern microbialite. Formation model via organic matrices (Lizard Island, Great Barrier Reef, Australia). *Bull. Inst. Océanogr. Monaco*, 14: 237–263, 1995.

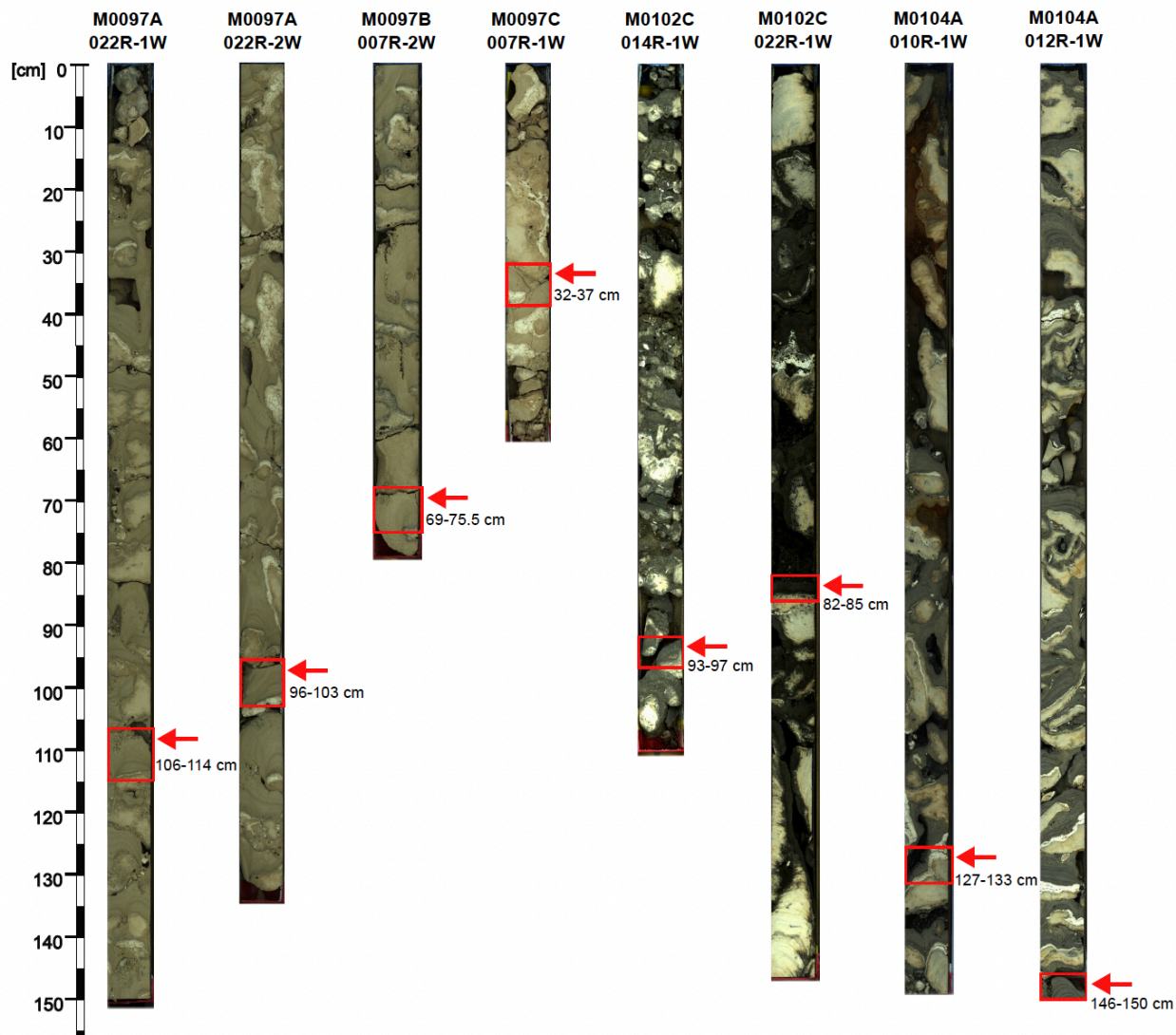
- Reitner, J., Thiel, V., Zankl, H., Michaelis, W., Wörheide, G., and Gautret, P.: Organic and biogeochemical patterns in cryptic microbialites. In *Microbial sediments* (pp. 149-160). Berlin, Heidelberg: Springer Berlin Heidelberg, 2000.
- 570 Ribes, M., Coma, R., Atkinson, M.J., and Kinzie, R.A.III: Sponges and ascidians control removal of particulate organic nitrogen from coral reef water, *Limnol. Oceanogr.*, 50(5), 2005, 1480–1489, 2005.
- Riding, R.: Microbial carbonate abundance compared with fluctuations in metazoan diversity over geological time. *Sedimentary Geology*, 134(1–2), 13–26, 2000a.
- 575 Riding, R.: Microbial carbonates: the geological record of calcified bacterial-algal mats and biofilms. *Sedimentology*, 47: 179-214, 2000b.
- Riding, R.: Microbial carbonate abundance compared with fluctuations in metazoan diversity over geological time. *Sedimentary Geology*, 185(3–4), 229–238, 2006.
- Riding, R.: Microbialites, stromatolites, and thrombolites. In *Reefs in Time and Space: The History and Evolution of the Reef-Building Biota* (pp. 103–120), 2011.
- 580 Riding, R. and Awramik, S.M. (Eds.): *Microbial Sediments*. Springer Verlag, Heidelberg, 331 p., 2000.
- Riding, R., Liang, L., and Braga, J.C.: Millennial-scale ocean acidification and late Quaternary decline of cryptic bacterial crusts in tropical reefs. *Geobiol.*, 12, 387-405, 2014.
- Riker-Coleman, K., Gallup, C., Clague, D., Webster, J.M., Edwards, L., and Cheng, H.: New 230Th ages from the – 400 m reef of northwestern Hawaii. *Eos, Transactions of the American Geophysical Union*, 86(52): PP21C-1574. <https://abstractsearch.agu.org/meetings/2005/FM/PP21C-1574.html>, 2005.
- 585 Robles-Fernández, A., Areias, C., Daffonchio, D., Vahrenkamp, V. C., and Sánchez-Román, M.: The Role of Microorganisms in the Nucleation of Carbonates, Environmental Implications and Applications. *Minerals*, 12(12), 1562. <https://doi.org/10.3390/min12121562>, 2022.
- 590 Salas-Saavedra, M., Dechnik, B., Webb, G.E., Webster, J.M., Zhao, J.-X., Nothdurft, L.D., Clark, T.R., Graham, T., and Duce, S.; Holocene reef growth over irregular Pleistocene karst confirms major influence of hydrodynamic factors on Holocene reef development. *Quaternary Science Reviews*, 180, 157–176. <https://doi.org/10.1016/j.chemgeo.2022.120871>, 2018.
- Sanborn, K.L., Webster, J.M., Yokoyama, Y., Dutton, A., Braga, J.C., Clague, D.A., Paduan, J.B., Wagner, D., Rooney, J.J., and Hansen, J.R.: New evidence of Hawaiian coral reef drowning in response to meltwater pulse-1A. *Quaternary Science Reviews*, 175:60–72. <https://doi.org/10.1016/j.quascirev.2017.08.022>, 2017.
- 595 Sanfilippo, K., Timm, O.E., Frazier, A.G., and Giambelluca, T.W.: Effects of systematic predictor selection for statistical downscaling of rainfall in Hawai'i. *International Journal of Climatology*, 44(2), 571–591. <https://doi.org/10.1002/joc.8345>, 2024.
- Schubert, J.K. and Bottjer, D.J.: Early Triassic stromatolites as post-mass extinction disaster forms: *Geology*, v. 20, p. 883–886, 1992.
- 600

- Séard, C., Camoin, G., Yokoyama, Y., Matsuzaki, H., Durand, N., Bard, E., Sepulcre, S., and Deschamps, P.: Microbialite development patterns in the last deglacial reefs from Tahiti (French Polynesia; IODP Expedition #310): Implications on reef framework architecture. *Marine Geology*, 279, 63-86, <https://doi.org/10.1016/j.margeo.2010.10.013>, 2011.
- Shirokova, L.S., Mavromatis, V., Bundeleva, I.A., Pokrovsky, O.S., Bénézech, P., Gérard, E., Pearce, C.R., and Oelkers, E.H.:
 605 Using Mg Isotopes to Trace Cyanobacterially Mediated Magnesium Carbonate Precipitation in Alkaline Lakes. *Aquat Geochem* 19, 1–24. <https://doi.org/10.1007/s10498-012-9174-3>, 2013.
- Stolz, J., Reid, R.P., Visscher, P., Decho, A., Norman, R., Aspden, R., Bowlin, E., Franks, J., Foster, J., Paterson, D., Przekop, K., Underwood, G., and Prufert-Bebout, L.: The Microbial Communities of the Modern Marine Stromatolites at Highborne Cay, Bahamas. *Atoll Research Bulletin*. 567. 10.5479/si.00775630.567.1, 2009.
- 610 Swart, P.K. and Melim, L.A.: The origin of dolomites in Tertiary sediments from the margin of Great Bahama Bank. *Journal of Sedimentary Research*, 70, 738–748, 2000.
- Szilagyi, Z., Webster, J.M., Patterson, M.A., Hips, K., Riding, R., Foley, M., Humblet, M., Yokoyama, Y., Liang, L., Gischler, E., Montaggioni, L., Gherardi, D., Braga, J.C.: Controls on the spatio-temporal distribution of microbialite crusts on the Great Barrier Reef over the past 30,000 years: *Marine Geology*. <https://doi.org/10.1016/j.margeo.2020.106312>, 2020.
- 615 Taylor, B.: Shoreline slope breaks revise understanding of Hawaiian shield volcanoes evolution. *Geochemistry, Geophysics, Geosystems*, 20(8):4025–4045. <https://doi.org/10.1029/2019GC008436>, 2019.
- van Lith, Y., Warthmann, R., Vasconcelos, C., and McKenzie, J.A.: Sulphate-reducing bacteria induce low-temperature Ca-dolomite and high Mg-calcite formation. *Geobiology*, 1, 71–79, 2003.
- Visscher, P.T. and Stolz, J.F.: Microbial mats as bioreactors: populations, processes, and products. *Palaeogeography, Palaeoclimatology, Palaeoecology*, 219(1–2), 87–100, 2005.
- 620 Vogt, C., Lauterjung, J., and Fischer, R.X.: Investigation of the clay fraction (<2 µm) of the clay mineral society reference clays. *Clays and Clay Minerals*, 50(3): 388-400, 2002.
- Watts, A.B.: An analysis of isostasy in the world's oceans, 1. Hawaiian-Emperor Seamount Chain. *Journal of Geophysical Research: Solid Earth*, 83(B12):5989–6004. <https://doi.org/10.1029/JB083iB12p05989>, 1978.
- 625 Webb, G.E.: Was Phanerozoic reef history controlled by the distribution of nonenzymatically secreted reef carbonates (microbial carbonate and biologically induced cement)? *Sedimentology*, v. 43, p. 947–971, 1996.
- Webb, G.E.: Quantitative Analysis and Paleoecology of Earliest Mississippian Microbial Reefs, Gudman Formation, Queensland, Australia: Not Just Post-Disaster Phenomena. *Journal of Sedimentary Research*. 75. 875-894. 10.2110/jsr.2005.068, 2005.
- 630 Webb, G.E. and Kamber, B.S.: Trace Element Geochemistry as a Tool for Interpreting Microbialites. In: Golding, S., Glikson, M. (eds) *Earliest Life on Earth: Habitats, Environments and Methods of Detection*. Springer, Dordrecht. https://doi.org/10.1007/978-90-481-8794-2_6, 2010.
- Webb, G.E. and Jell, J.S.: Cryptic microbialite in subtidal reef framework and intertidal solution cavities in beachrock, Heron Reef, Great Barrier Reef, Australia: preliminary observations, in Neuweiler, F., Reitner, J. & Monty, C. (eds.)

- 635 Biosedimentology of microbial buildups, IGCP Project No. 380, Proceedings of 2nd Meeting Göttingen/Germany 1996. *Facies*, 36, 219-223, 1997.
- Webb, G.E., Baker, J.C. and Jell, J.S.: Inferred syngenetic textural evolution in Holocene cryptic reefal microbialites, Heron Reef, Great Barrier Reef, Australia. *Geology* v. 26, p. 355–358, 1998.
- Webster, J.M., Clague, D.A., Riker-Coleman, K., Gallup, C., Braga, J.C., Potts, D., Moore, J.G., Winterer, and E.L., Paull, 640 C.K.: Drowning of the -150m reef off Hawaii: a casualty of global meltwater pulse 1A? *Geology*, 32(3):249– 252. <https://doi.org/10.1130/G20170.1>, 2004.
- Webster, J.M., Wallace, L.M., Clague, D.A., Braga, J.C.: Numerical modeling of the growth and drowning of Hawaiian coral reefs during the last two glacial cycles (0–250 kyr). *Geochemistry, Geophysics, Geosystems*, 8(3):Q03011. <https://doi.org/10.1029/2006GC001415>, 2007.
- 645 Webster, J.M., Braga, J.C., Clague, D.A., Gallup, C., Hein, J.R., Potts, D.C., Renema, W., Riding, R., Riker-Coleman, K., Silver, E., and Wallace, L.M.: Coral reef evolution on rapidly subsiding margins. *Global and Planetary Change*, 66(1–2):129–148. <https://doi.org/10.1016/j.gloplacha.2008.07.010>, 2009.
- Webster, J.M., Ravelo, A.C., and Grant, H.L.J.: Expedition 389 Scientific Prospectus: Hawaiian Drowned Reefs. International Ocean Discovery Program. <https://doi.org/10.14379/iodp.sp.389.2023>, 2023.
- 650 Webster, J.M., Ravelo, A.C., Grant, H.L.J., and the Expedition 389 Scientists: Expedition 389 Preliminary Report: Hawaiian Drowned Reefs. International Ocean Discovery Program. <https://doi.org/10.14379/iodp.pr.389.2024>, 2024.
- Webster, J.M., Ravelo, A.C., Grant, H.L.J., and the Expedition 389 Scientists: Hawaiian Drowned Reefs. Proceedings of the International Ocean Discovery Program, 389: College Station, TX (International Ocean Discovery Program). <https://doi.org/10.14379/iodp.proc.389.2025>, 2025.
- 655 Westphal, H., Heindel, K., Brandano, M., Peckmann, J.: Genesis of microbialites as contemporaneous framework components of coral reefs, deglacial of Tahiti (IODP 310). *Facies* 56, 337-352. <https://doi.org/10.1007/s10347-009-0207-3>, 2010.
- White, B., Kurkju, K.A., Curran, H.A., and Besom, K.A.: Shallowing-upward sequence in a Pleistocene coral reef and associated facies, San Salvador, Bahamas. *AAPG Bulletin*, 68, 539–539, 1984.
- Zhang, H.S., Dai, M.-Y., Qi, Y.-A., Han, L.-L., Yin, Z.-L., Chen, S.-H., and Lin, L.-B.: *Girvanella* fossils from the 660 Phanerozoic: Distribution, evolution and controlling factors. *J. Palaeogeogr.*, 13, 924–938, 2024.
- Zhu, Y. and Dittrich, M.: Carbonate precipitation through microbial activities in natural environments, and their potential in biotechnology: a review. *Front. Bioeng. Biotechnol.*, 4, 4, 2016).

Appendix A: Line scans of H2-terrace reef cores studied here by means of SEM. Core width is 7.2 cm.

Fig. A1

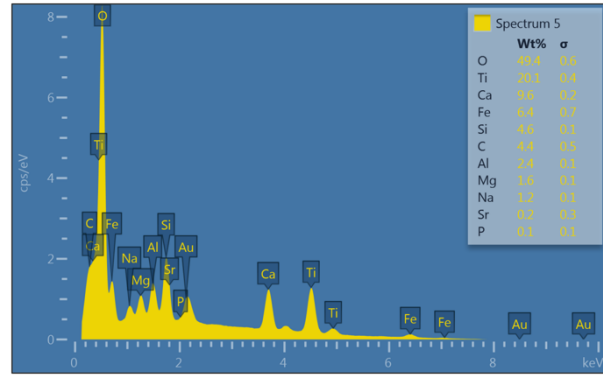
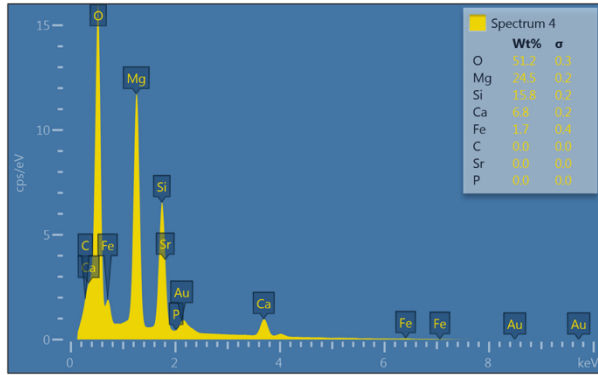
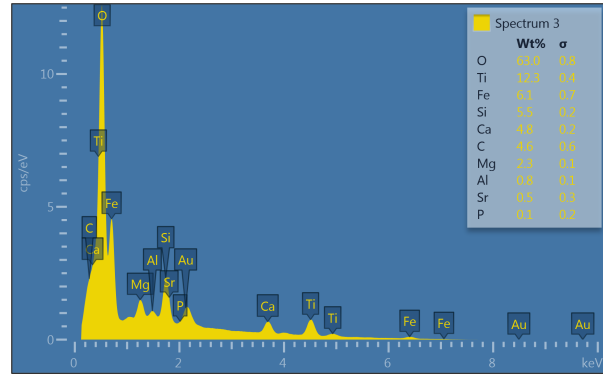
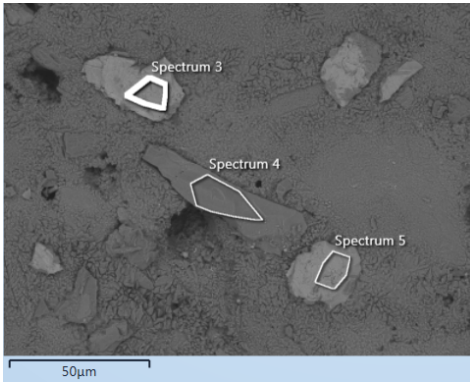


Appendix B: Samples from IODP Expedition 389 studied here.

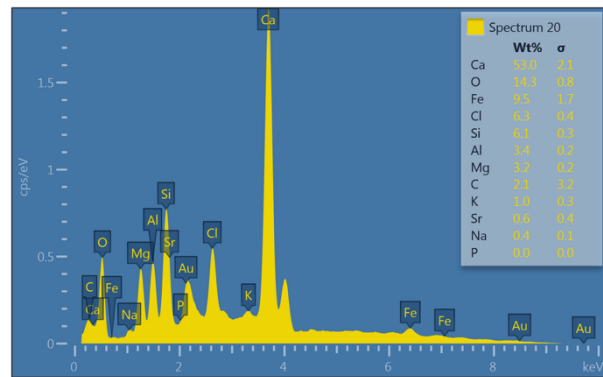
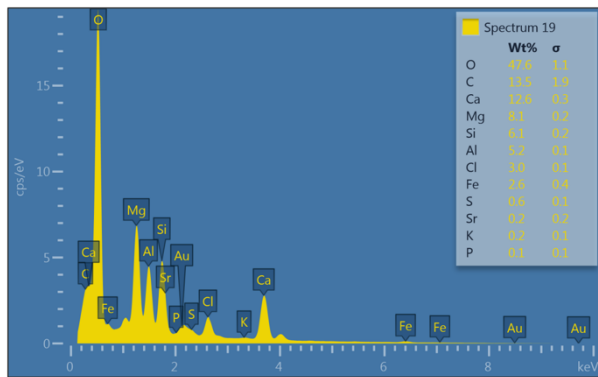
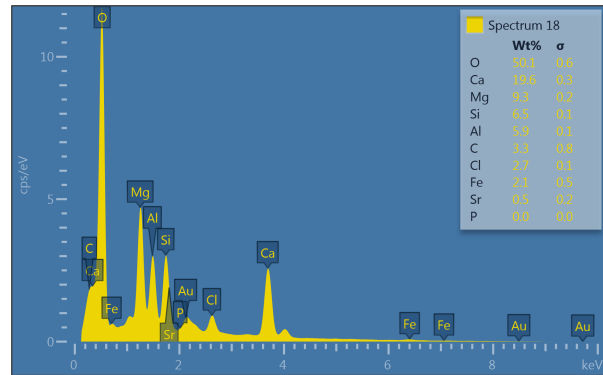
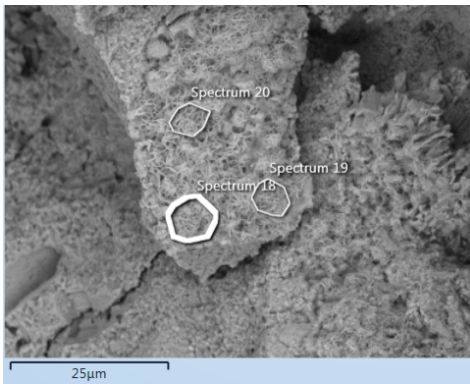
Table B1

Side of Island	Site	Sample ID	Estimated age range (Webster et. al. 2025)	SEM	XRD
Windward, humid	Kohala	M0102_C_014R_1W 93 - 97 cm	171-225 ky	X	X
Windward, humid	Kohala	M0102_C_022R_1W 82-85 cm	171-225 ky	X	X
Windward, humid	Hilo	M0104_A_010R_1W 127-133 cm	130-159 ky	X	X
Windward, humid	Hilo	M0104_A_012R_1W 146-150 cm	130-159 ky	X	X
Windward, humid	Hilo	M0104_A_013R_11W_11-20 cm	130-159 ky		X
Leeward, arid	Kawaihae	M0097_A_022R_1W 106 -114 cm	133-150 ky	X	X
Leeward, arid	Kawaihae	M0097_A_022R_2W 96-103 cm	133-150 ky	X	X
Leeward, arid	Kawaihae	M0097_B_007R_2W 69-75.5 cm	133-150 ky	X	X
Leeward	Kawaihae	M0097_B_007A_2W_93-76.5 cm	133-150 ky		X
Leeward	Kawaihae	M0097_C_007R_1W 32-37 cm	133-150 ky	X	X

Figure C1: EDX spectra of entrapped non-carbonate grains; sample M0104A-012R-1, 146-150 cm.



680 Fig. C2: EDX spectra of flaky minerals, sample M0104A-012R-1, 146-150 cm.



Appendix D: Mineralogical composition according to XRD results in %. HMC indicates high-Magnesium calcite.

Table D1

Side of Island	sample	HMC	Aragonite	Anorthite	others
Windward	M102C_014R_1W_93-97	62	31	4	3 (Muscovite, Brushite)
Windward	M102C-022R-1W_82-85	79	9	7	4 (Richterite, Gypsum)
Windward	M104A-010R-21W_124-133	81	13	3	3 (Quartz)
Windward	M104A-012R_1W_146-150	78	15	0	7 (Quartz, Ilmenite, Ramsdellite)
Windward	M104A-013R-11W_11-20	80	13	7	0
Leeward	M097A-022R_1W_106-114	87	12	0	1 (Huntite)
Leeward	M097A_022R_2W_96-103	88	12	0	0
Leeward	M097B-007A-2W_93-76.5	89	9	0	2 (Huntite, Pyrolusite)
Leeward	M097B_007R_2W_69-75.5	81	13	0	6 (Calcite)
Leeward	M097C_007R_1W_32-37	81	19	0	0